ABSTRACT

Title of Thesis: PROTEIN ENGINEERING APPROACHES TO IMPROVE THE THERAPEUTIC POTENTIAL OF HISTATIN-5 FOR CANDIDA ALBICANS INFECTIONS

Jesse A Leissa, Master of Science, 2019

Thesis Directed By: Professor Amy J. Karlsson, Department of Chemical and Biomolecular Engineering

The salivary peptide histatin 5 has been studied as a novel therapeutic to address rising drug resistance and limited therapeutics for treating infections caused by the fungal pathogen *Candida albicans*. While histatin 5 possesses antifungal activity, degradation from secreted aspartic proteases produced by *C. albicans* hinders its potential. To develop a strategy that will identify variants of histatin 5 with improved proteolytic stability, the peptide was integrated into a yeast surface display system, and the proteolytic degradation conditions were optimized to improve the resolution between proteolytically stable (K11RK17R) and proteolytically susceptible (K13L) variants. Additionally, histatin 5 and K11RK17R were embedded in polyelectrolyte multilayer films (PEMs) to investigate their ability to prevent biofilm formation on surfaces. Significant biofilm formation was prevented at high

concentrations of K11RK17R, while histatin 5 encouraged biofilm formation. My results support the therapeutic potential of histatin 5 and will enable the design of improved peptide-based therapeutic approaches.

PROTEIN ENGINEERING APPROACHES TO IMPROVE THE THERAPEUTIC POTENTIAL OF HISTATIN-5 FOR CANDIDA ALBICANS INFECTIONS

by

Jesse Alton Leissa

Thesis submitted to the Faculty of the Graduate School of the
University of Maryland, College Park, in partial fulfillment
of the requirements for the degree of
Master of Science
2019

Advisory Committee:
Professor Amy J. Karlsson, Chair
Professor Ganesh Sriram
Professor Srinivasa Raghavan

Acknowledgements

First and foremost, I would like to thank my advisor, Dr. Amy Karlsson, for her guidance, support, and for giving me the opportunity to perform this research in her laboratory. Being able to work under and learn from Dr. Karlsson has been a priceless, enjoyable experience that has helped me become a better student and researcher.

I would also like to thank the other graduate students of the Karlsson Lab: Sayanee Adhikari and Mahdi Ghorbani, for constantly offering to help me in my laboratory efforts and for being a constant resource for creative brainstorming. Both of you have been good friends that I can always count on to embody the definition of good work ethic and leaders. The completion of this work would also not have been possible without assistance from Thomas Matherly, who was instrumental in helping me with the molecular cloning and optimization work performed on the yeast surface display system. Your humor made working in the lab an unforgettable, fun experience.

Outside of the Karlsson lab, there are also several other individuals who have played key roles in this research that I want to thank. I want to thank Haleigh Eppler for showing me the ropes with regards to the construction of the polyelectrolyte multilayer films and troubleshooting assistance throughout that project as well as the other members of the Jewell lab for their general assistance. I would also like to thank John Abrahams for his assistance in the FabLab and Kenneth Class for this guidance in setting up and analyzing the flow cytometry data.

I would also like to thank my parents, Brad and Dorothy Leissa, for their unwavering support and unconditional love. You both have played major roles in molding me into the capable, independent man that I am proud to have become. I am very proud to be your son. My sisters, Sophia and Greta, have also been very supportive throughout my life, for which I owe them thanks. I am thankful to have two great sisters that I can rely on to have my back.

Last, but not least, I would like to thank my friends for helping me maintain a well-balanced life style and for helping me maintain my sanity throughout my undergraduate and graduate academic careers. Thank you for encouraging me to take pride in my work and for helping me relieve stress when I need it most.

Table of Contents

List of Tables

List of Figures

Chapter 1: Introduction

Chapter 2: Engineering Enhanced Proteolytic Stability in Histatin 5 with Yeast Surface Display

Chapter 3: Incorporating Antifungal Peptides into Polyelectrolyte Multilayer Films (PEMs)

List of Abbreviations

AIDS	= Acquired immunodeficiency syndrome
ANOVA	= Analysis of variance
ATCC	= American type culture collection
C. albicans	= *Candida albicans*
C. auris	= *Candida auris*
C. glabrata	= *Candida glabrata*
CFU	= Colony forming units
FACS	= Fluorescence-activated cell sorting
GPI	= Glycosylphophtidylinositol
HA	= Human influenza hemagglutinin
HIV	= Human immunodeficiency virus
HSCT	= Hematopoietic stem cell transplantation
LBL	= Layer-by-layer
NaPB	= Sodium phosphate
OD_{600}	= Optical density at 600 nm
PAH	= poly(allylamine)
PBS	= Phosphate buffered saline
PEI	= polyethylenimine
PEM	= Polyelectrolyte multilayer film
PGA	= poly-L-glutamic acid
PLL	= poly-L-lysine
POI	= protein/peptide of interest
PSS	

	= poly(styrenesulfonate)
ROS	= Reactive oxygen species
Sap	= Secreted aspartic protease
ScFv	= Single-chain variable fragment
SD-CAA Media	= Synthetic dextrose-casamino acids media
SG-CAA Media	= Synthetic galactose-casamino acids media
SPS	= sulfonated polystyrene
TBS	= Tris-buffered saline
TBST	= Tris-buffered saline with Tween
Y-PER	= Yeast protein extraction reagent
YESS	= Yeast endoplasmic reticulum sequestration system
YPD Media	= Yeast-peptone-dextrose media

Chapter 1: Introduction

1.1 Clinical Relevance of C. albicans

Candida albicans is a fungal pathogen within the *Candida* genus of ubiquitous, yeasts that are naturally associated with the flora of the skin, intestinal tract, and genitourinary tract of healthy individuals [1]. Commensal in nature, *C. albicans* lives within these microbiomes along with other *Candida* species without harm until an individual's immunity is compromised and the risk of opportunistic infection increases. *Candida* can then reversibly transition from a yeast to hyphal state (Figure 1.1) [2]. In hyphal form, *C. albicans* can invade local tissue and colonize the surfaces of medical devices such as implants, dentures, and catheters, causing a range of responses from minor candidemia symptoms to severe sepsis [3]. *C. albicans* is the most prevalent species of *Candida* in these infections, which is attributed to its high adaptability to stressful and unfavorable environments [3, 4]. With this in mind, *C. albicans* represents a significant health risk to those undergoing chemotherapy [5], recipients of solid-organ transplants [6] or hematopoietic stem cell transplants (HSCTs) [7], and individuals with diabetes [8], HIV/AIDS infections [9], and pregnant women [10]. Additionally, contraction of a *C. albicans* infection can pose a significant financial burden on patients as adequate treatment can result in an average increase in total hospital charges and cost of hospitalization by $6,000-$29,000 and $3,000-$22,000 respectively and extend a patient's stay by 3-13 days [11]. However,

treatment options for these infections is fortunately well established and can be usually mitigated with early detection and prophylactic treatment.

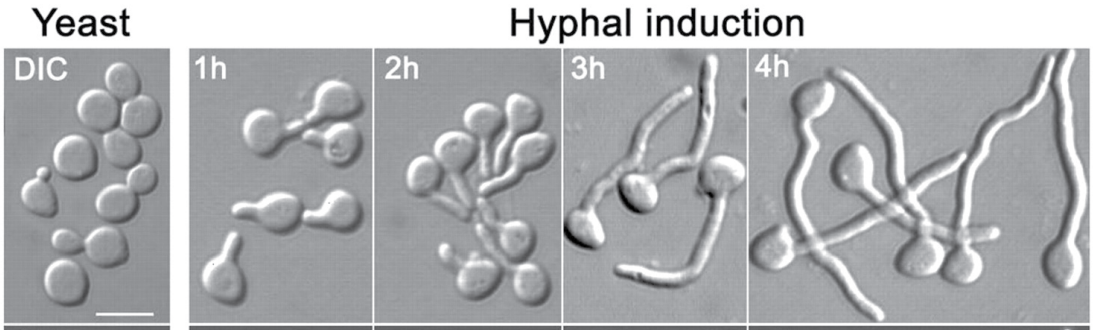

Figure 1.1: Yeast and Hyphal States of *C. albicans*. Figure modified from reference [2]. Used with permission. Yeast form of C. albicans is shown in the left-most panel followed by developing stages of hyphal formation in the remaining panels (left to right). Scale bar represents 5 μm.

To treat *C. albicans* infections, echinocandins (caspofungin and micafungin) are currently used for primary treatment with high survival rates [3, 12]. This class of small molecule drugs target *C. albicans* by inhibiting the synthesis of β-(1,3)-glucan, a major structural component of the fungal cell wall, and compromise the structural integrity of the cell [13]. However, repeat treatment with this class of therapeutics has resulted in the emergence of echinocandin-resistant *C. albicans*, which gain resistance through the upregulation of chitin synthesis to repair damage caused by echinocandins and strengthen the cell wall [13]. The emergence of echinocandin-resistant *C. albicans* was first reported in 2005 and continues to rise, currently comprising 2-3% of all *C. albicans* infections with approximately 36% of them displaying resistance towards azoles as well [14].

Azoles (fluconazole, itraconazole, and voriconazole) are another class of efficacious antifungal, small molecule drugs that are also used for either primary or

secondary (i.e. step-down) treatment for both topical and systemic *C. albicans* infections [3, 12, 15]. While there are differing opinions as to whether echinocandins or azoles are better for treatment, the azoles are more commonly used due to their highly demonstrated efficacy [3, 15], low cost [16], and more convenient and adaptable dosing regimen, which ensures higher patient compliance [15]. Similar to echinocandins, this class of therapeutics target *C. albicans* by inhibiting the synthesis of the sterol ergosterol. Azoles inhibit 14α-demethylase encoded by the gene ERG11 [16]. Therefore, it is not surprising that azole-resistant *C. albicans* strains have also emerged, utilizing efflux pumps, mutations in the ERG11 gene, and development of bypass signaling pathways to overcome the stress imparted by azoles [17]. The heavy reliance on this class of therapeutics and high incidence of resistant isolates has made azole-resistant *C. albicans* a serious threat to public health, making it onto the report of antibiotic resistance threats published by the Centers for Disease Control and Prevention in 2013 [18]. In these cases, where azole and echinocandin resistance are observed, amphotericin B is often utilized to treat these persistent infections.

Amphotericin B is a third, potent treatment option used for secondary treatment of *C. albicans* infections or primary treatment in low resource areas [12]. Amphotericin B targets *C. albicans* by selectively binding to ergosterol in the cell membrane and inducing pore formation followed by rapid cell death [19]. Isolates of *C. albicans* that are resistant to amphotericin B have been reported in select cases, and resistance occurs when the cell turn off the production of C-5 sterol desaturase and lanosterol 14α-demethylase through ERG3 and ERG11, respectively, leading to changes in their membrane composition; however, the relative amount of observed

resistance has remained stagnant over the past 50 years [19, 20]. Therefore, amphotericin B represents a promising therapeutic for the continued treatment of drug-resistant *C. albicans*. However, the reason this drug is not used in primary treatment is because of its inherent kidney toxicity [19, 21, 22, 23]. Combinatorial therapy of amphotericin B and fluconazole have been shown to reduce kidney toxicity with efficacious performance against azole-resistant *C. albicans* [21]. Additionally, lipid (Abelcet) and liposomal (AmBisome) formulations of amphotericin B have been shown to reduce these toxic side effects and increase its safety profile [22, 23]. However, the high cost of these formulations is responsible for their low utility in the clinical setting [24]. With this in mind, reduced sensitivity to amphotericin B remains difficult to treat and is also becoming more of an issue in *Candida* infections caused by non-albicans species.

In addition to *C. albicans*, the rise of international, multi-drug resistance has also been documented in *C. auris* [25, 26, 27] and *C. glabrata* [26] with alarming global incidence. In both cases, multiple incidence of fluconazole resistant strains has been reported with variable sensitivity to echinocandins, azoles, and amphotericin B, which make them difficult to treat [26, 27]. Furthermore, both inter- and intra-transmission of multi-drug resistant *C. auris* infections have been denoted, giving rise to its spread amongst patients [25, 27]. With this in mind, there is a demand for novel therapeutics that can expand the currently limited arsenal of treatment options and address the growing presence of multi-drug resistant strains of *C. albicans* and emerging non-albicans species.

1.2 Novel Antifungal Therapeutics

Given the growing presence of fluconazole-resistant *C. albicans* as well as multi-drug resistant strains, novel therapeutics and strategies are required to contain these threats and support the treatment of these infections when current methods fail. In response to this, antifungal peptides represent an advantageous alternative due to their consistently high levels of safety, tolerance, and efficacy, which distinguishes them from small molecule drug alternatives [28]. Additionally, due to the natural origin of these therapeutics, antifungal peptides enjoy an inherently selective mode of antifungal/bacterial action, making them great platforms for therapeutics [29]. The threat of drug-resistance to this class of therapeutics is also less than that for small molecules as their rapid fungicidal activity and cell-wall specificity minimizes the opportunity for adaptation [30]. However, antifungal peptides, as well as other peptide therapeutics, are currently significantly more expensive to manufacture compared to the small molecule drugs currently utilized, preventing them from becoming widely used in the clinic [31]. For example, it is generally estimated that the production cost of a 5 kDa peptide will exceed the production of a 500 Da small molecule by more than 10-fold assuming the peptide is produced via solid-phase synthesis, which is currently the most mature form of technology for the production of peptides [31]. Despite this fact, antifungal peptides remain an important area for therapeutic development due to their promising safety profile, lack of off-target binding, and flexible pharmacokinetic profile, which can be adjusted with protein engineering methods [32]. While many antifungal peptides are currently being

studied, one that has received noticeable attention with regards to therapeutic development is histatin 5.

Histatin 5 is a natural, histidine-rich, cationic, salivary peptide part of the innate immune system with strong antifungal activity for *C. albicans* and other foreign microbes [33]. A member of a larger family of histatin peptides secreted from the human parotid gland, histatin 5 is 24 amino acids long and exhibits the highest fungicidal activity against *C. albicans* of the histatins [34]. Unlike many antifungal peptides, which target the cell wall and cause pore formation to induce cell death, histatin 5 binds to the cell wall protein and glycans and utilizing influx pumps, Dur3 and Dur31, to traverse the cell membrane [33, 35], which is illustrated in Figure 1.2. Inside, reactive oxygen species (ROS) are generated by histatin 5 in the mitochondria, leading to stress response and rapid cell death [33, 35]. In response to this, *C. albicans* has been reported to reduce the cytosolic concentration of histatin 5 by removing the peptide through the efflux pump Flu-1 as a means of resistance [35, 36, 37]. Fortunately, this phenomenon has been limited to Flu-1 and associated efflux pumps and has not been observed through mutations or down regulation of Dur3 or Dur31, which is most likely due to the pathogen's reliance on these pumps for viability and their unique role in polyamine intake [37, 38, 39]. Despite this mechanism of natural resistance, histatin 5 has significant fungicidal activity for *C. albicans* and has been demonstrated as a promising therapeutic to treat vulvovaginal candidiasis [40], prevent *C. albicans* proliferation in a variety of pHs and ionic strengths [41] and display potency against fluconazole-resistance *C. albicans* [42].

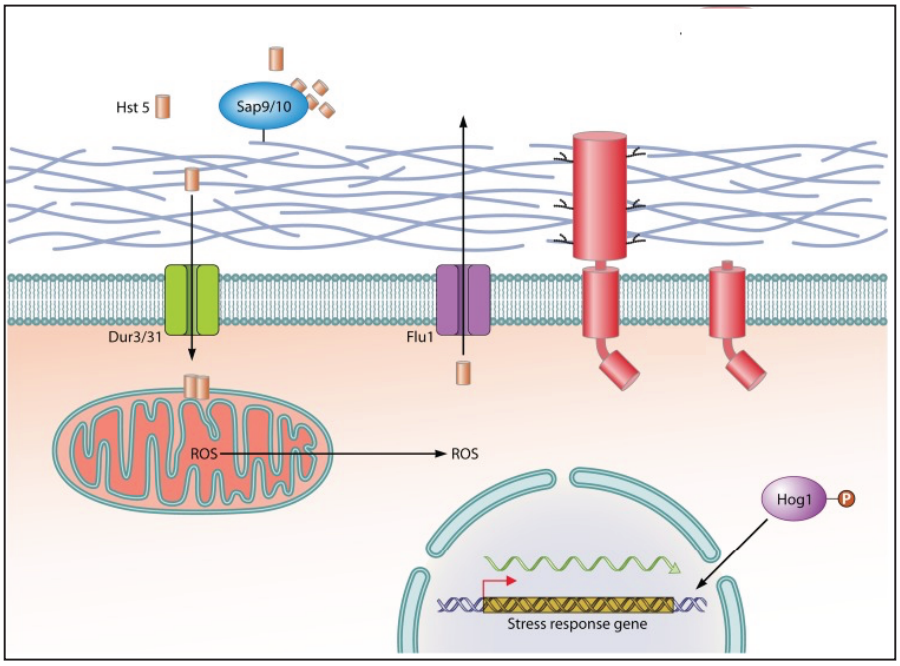

Figure 1.2: Transport of Histatin 5 into *C. albicans*. This figure was acquired from reference [35]. Used with permission. In this diagram, histatin 5 (orange cylinders) is shown entering the cytosol through the transmembrane Dur3/31 influx pumps and generating ROS species in the mitochondria. The efflux pump Flu1 is also shown releasing histatin 5 into the extracellular space.

Histatin 5 is also highly explored as a novel therapeutic because of its ability to reduce the pathogen's virulence factors: filamentation and biofilm formation [43]. This phenomenon is attributed to histatin 5's generation of stress response in *C. albicans*, which subsequentially reduces the hyphal growth and biofilm development through environmental signaling pathways [44]. Inhibiting biofilm formation is advantageous as it prevents infection as well as the colonization of *C. albicans* to medical devices [45]. Given this behavior, *C. albicans* is not likely to develop additional resistance to histatin 5, as the low doses required to prevent filamentation do not significantly challenge the viability of the cell [24, 46]. However, one virulence factor that histatin 5 cannot prevent, which poses a limitation to the

therapeutic index of histatin 5, are the secreted aspartic proteases (Saps) naturally generated by *C. albicans* which can degrade the peptide into less potent fragments.

1.3 Secreted Aspartic Proteases (Saps) Expressed by C. albicans

To aid in its virulence, *C. albicans* secretes a family of ten secreted aspartic proteases (Saps) that assist with infection by degrading cell surfaces and host immune proteins [47]. Among these ten aspartic proteases, Sap1 through Sap8 are fully secreted to the extracellular environment while Sap9 and Sap10 are anchored to the cell wall through a GPI-anchor or GPI proteins [48, 49]. The expression of each Sap is dependent upon the environmental conditions, such as local pH and the type of local tissue, and the morphological state of the cell [49]. For example, Sap1 through Sap3 are primarily expressed in the yeast cell state while Sap4 through Sap6 are more prevalent in its hyphal form in oral candidiasis [49]. Meanwhile, in the case of vulvovaginal candidiasis, Sap2 Sap9, and Sap10 are initially observed followed by Sap1, Sap4, and Sap5 in early stages of infection and Sap6 and Sap7 in later stages [49]. In both cases of oral and vulvovaginal candidiasis, Sap2, Sap5, Sap9, and Sap10 remains the most highly expressed protease [50]. Therefore, a host of possible SAPs are available for the degradation of endogenous and therapeutic antifungal peptides, which can limit the therapeutic potential of peptide-based antifungal agents.

The SAPs expressed by *C. albicans* possess a diverse range of substrate specificities, presenting a potent cocktail for the degradation of local proteins and peptides [51]. Sap1 through Sap6 and Sap8 preferentially degrade at positively charged (Arg and Lys) and large hydrophobic (Leu, Phe, and Tyr) amino acids while Sap7, Sap9 and Sap10 prefer Met, Arg, and His, respectively [51]. Additionally, Saps

possess a global specificity for Ala at the amino acid located directedly downstream of the primary amino acid site with the exception of Sap6, which prefers Tyr [52]. Therefore, designing therapeutic agents that are completely resistant to proteolytic degradation from all Saps can be a difficult task. An easier alternative involves identifying Saps with the most significant substrate activity or opportunity for degradation and engineering the peptide for high proteolytic stability with respect to these Saps. As a starting point, the degradation activity of Sap2 and Sap9 was investigated on histatin 5 due to their overall high expression and broadly covered specificity [53].

1.4 Prior Efforts to Increase the Proteolytic Stability of Histatin 5

Given that histatin 5 was significantly degraded by Sap2 (40% degraded) and Sap9 (60% degraded) [53], and both Saps possess promiscuous specificity [51], mutations were investigated for their ability to impact proteolytic stability [53]. The primary residues that were investigated were lysines due to an observed preference for cleaving this amino acid in histatin 5 [54]. Each of the lysines was substituted with either arginine or lysine [53]. From proteolytic degradation assays, the mutation K17R significantly increased the proteolytic stability and K13L decreased the proteolytic stability [53]. Most importantly, these mutations did not reduce the antifungal activity of the peptide. A double mutant, K11RK17R, was also found to further improve the proteolytic stability of histatin 5 beyond that imparted by each individual mutation [55]. Given these significant improvements, it begs the question that other sites can be explored and if further improvement can be imparted with other mutations. One way to investigate these possibilities is through directed evolution.

1.5 Directed Evolution as an Approach to Identify Variants with High Proteolytic Stability

Directed evolution, which mimics the process of natural selection, is an important approach used to improve the fitness properties of proteins and peptides for therapeutic applications. This involves introducing random variation throughout the gene for the peptide or protein of interest and subjecting the library to successive rounds of screening and mutagenesis, where a promising mutant or mutants isolated from a given round are used as the foundation for mutagenesis in the next round [56]. Iterations continue until a mutant(s) with the desired fitness for a desired property are identified [57].

This approach has been validated through the screening of mutations in the PK15 bicyclic peptide with improved inhibition of the intestinal protease plasma kallikrein (hPK), which degrades therapeutic peptides in this region [58]. Applying directed evolution through phage surface display, potent inhibitors were identified with inhibitory concentrations in the nM range with a consensus Xaa-Pro motif [58]. Additionally, directed evolution can be used to identify sites of preferential degradation, helping guide the usage of site-mutations to improve fitness. For example, McGlinchey et al. used directed evolution to elucidate the role of different cysteine cathepsins in the degradation of α-synuclein, a peptide associated with Parkinson's disease [59]. From these studies, significant degradation was observed with different cathepsins at different sites, allowing for the substrate specificity to be mapped [59]. With this in mind, random mutations could be implemented into histatin 5 to identify novel sites or mutations that can impart superior proteolytic stability.

1.6 Overview of Thesis

This thesis describes the work to optimize a yeast surface display system for histatin 5 to enable the effective screening of novel mutants for improved proteolytic stability and also investigates the potential of histatin 5 and K11RK17R to be coated on medical devices with polyelectrolyte multilayer films (PEMs) to treat oral candidiasis. In Chapter 2, histatin 5 and the variants K11RK17R and K13L are integrated into a yeast surface display platform and the degradation conditions are optimized to improve the resolution between proteolytically stable and susceptible peptides to assist in the future screening of a novel peptide library for improved proteolytic stability. In Chapter 3, a study is performed to investigate the potential for histatin 5 and K11RK17R to be incorporated into a surface coating for medical devices for the treatment of oral candidiasis. Finally, my conclusions and recommendations for future work are summarized in Chapter 4.

Chapter 2: Engineering Enhanced Proteolytic Stability in Histatin 5 with yeast Surface Display

2.1 Introduction

Yeast surface display is a cell surface display system developed in *Saccharomyces cerevisiae* that allows for the easy screening of a protein library for improved fitness properties. Initially designed by Boder and Wittrup in 1997 for the evolution of a human single-chain variable fragment (scFv) with improved binding affinity for its antigen (FITC-dextran) [60], this system represents a promising method for the protein engineering of mammalian and eukaryotic proteins. In yeast surface display, the protein of interest (POI) is targeted to the extracellular space as a part of a fusion to the cell wall by the cell-cell adhesions protein a-agglutinin 2 (Aga2) (Figure 2.1). Aga2 establishes a physical linkage to the cell wall with the help of a-agglutinin 1 (Aga1). Aga1 is covalently linked to 1,6-β-glucans in the yeast cell wall and Aga2 is connected to Aga1 by reduceable, disulfide bridges [60]. In the Aga2-POI fusion, the POI is covalently sandwiched between an upstream hemagglutinin antigen (HA) and downstream C-Myc epitope tags for quantification of display [60]. With this design, the phenotypic properties of the protein of interest can be physically traced back to the gene that produced it, providing the phenotype-genotype linkage characteristic of cell surface display methods [61].

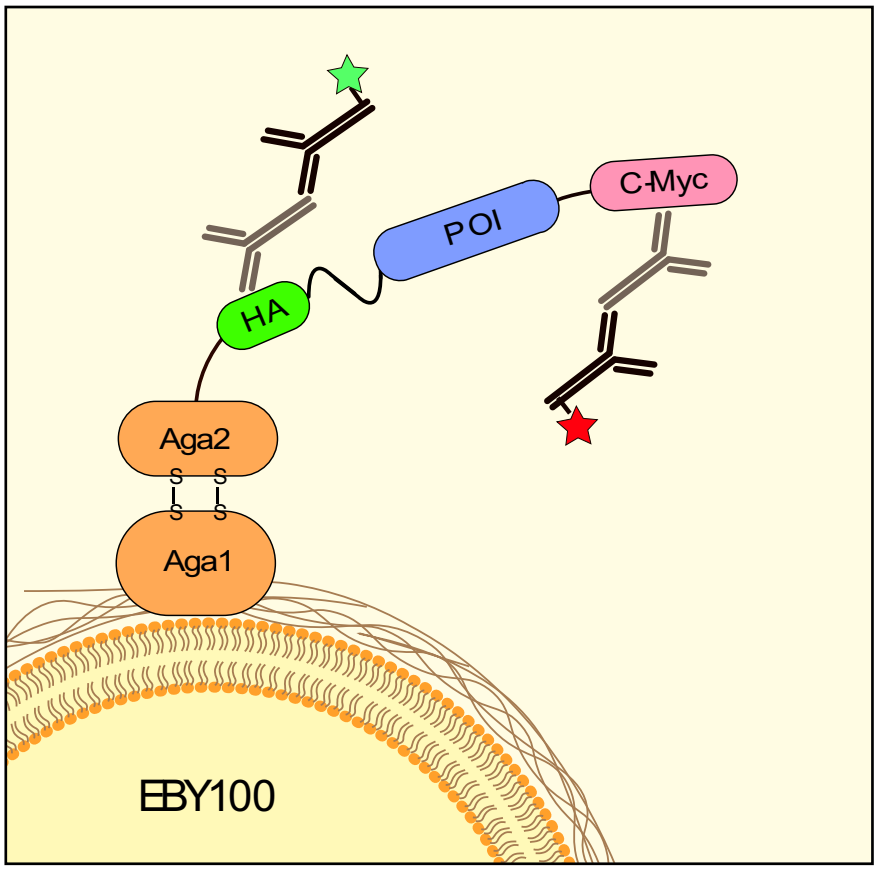

Figure 2.1: Schematic Illustration of Yeast Surface Display in Yeast. A terminal 10-residue epitope tag (C-Myc) is fused to the c-terminus of the protein of interest (POI), allowing detection of the whole fusion display. A flexible polyglycine-serine linker $(G_4S)_3$ covalently links the POI to the 9-residue HA epitope tag, allowing detection of the fusion display in the case of POI degradation. Upstream, the Aga2 protein subunit of a-agglutinin is bound to the Aga1 protein subunit through two disulfide bridges, anchoring the fusion protein to the cell wall.

Compared to other cell surface display methods such as bacterial and phage, yeast surface display possesses a competitive advantage given the larger size of the yeast cell (5-10 μm) compared to that of *E. coli* (1 μm) and phage (20-200 nm). This allows yeast to express significantly more fusion proteins (approximately $1 \times 10^4 - 1 \times 10^5$ fusions/cell), ensuring sufficient access for interrogation of the desired property [60, 62]. In terms of the library size, yeast surface display is able to accommodate ~10^{10} unique variants, which is similar to that of bacterial and phage display and is

only dwarfed by *in vitro* ribosome and mRNA screening platforms due to the transformation limitation needed to introduce the gene of interest into the yeast cells [62, 63]. While not relevant to work with histatin 5, it is also worth mentioning that yeast surface display is capable of expressing mammalian proteins with correct post-translational modifications and glycosylation patterns, allowing it to be used for the development of mammalian proteins and antibody domains [62].

Given the numerous advantages present in yeast surface display, this technology has been utilized in several different applications since its genesis, including epitope mapping [64, 65], cell adhesion engineering [65], and the identification of protein-protein interactions [64]. Additionally, in terms of proteolytic applications, yeast surface display has been used to map substrate selectivity of the tobacco etch virus protease and enhance the selectivity by 5,000 – 10,000-fold [64] and to develop potent protease inhibitors for human tissue kallikrein proteases [66] and trypsin [67]. Furthermore, yeast surface display has improved the proteolytic stability of the human amyloid precursor protein Kunitz protease inhibitor domain (APPI) in the presence of mesotrypsin, increasing its proteolytic stability by 83-fold [68]. With this in mind, yeast surface display is a promising tool that can be used to improve the proteolytic stability of histatin 5 and improve its therapeutic potential.

2.2 Materials and Methods

2.2.1 Peptides

The peptides utilized in this chapter can be found in Table 2.1 and were incorporated into the yeast surface display fusion using primers (Table 2.2), as described in section 2.2.3.

Table 2.1: Peptides Integrated into Yeast Surface Display

Peptide	Sequence*	MD (Da)	Net Charge**
Histatin 5	D S H A K R H H G Y K R K F H E K H H S H R G Y	3036	+12
K11RK17R	– – – – – – – – – – R – – – – – R – – – – – – –	3092	+12
K13L	– – – – – – – – – – – – R – – – – – – – – – – –	3021	+11

*Dashes indicate unchanged amino acids previously found in parent peptide.
**Net charge (pH 7.0) is calculated only from the amino acid side chains and does not include the N-terminal amine.

2.2.2 Strains and Culture Conditions

The *S. cerevisiae* strain EBY100 was purchased from the American Type Culture Collection (ATCC). Cells were first inoculated from a synthetic dextrose-casamino acids (SD-CAA) yeast minimal media (20g/L dextrose, 6.7 g/L yeast nitrogen base, 5.0 g/L casamino acids, 5.4 g/L Na_2HPO_4, 8.56 g/L $NaH_2PO_4{\cdot}H_2O$, 182 g/L sorbitol, pH 6.0) agar plate into 7.5 mL of SD-CAA media (20g/L dextrose, 6.7 g/L yeast nitrogen base, 5.0 g/L casamino acids, 10.4 g/L sodium citrate, 7.4 g/L citric acid monohydrate, pH 4.5) and grown overnight (≈24 h) at 30°C while shaking at 230 rpm. The overnight cell culture was subsequentially subcultured into 7.5 mL of fresh SD-CAA media (20g/L dextrose, 6.7 g/L yeast nitrogen base, 5.0 g/L casamino acids, 10.4 g/L sodium citrate, 7.4 g/L citric acid monohydrate, pH 4.5) at a starting optical density measured as the absorbance at 600 nm (OD_{600}) of 0.1. The culture was

grown at 30°C while shaking at 230 rpm until the OD_{600} reached 2.0-3.0 (≈8-10 h). The cell culture was centrifuged at 3,000 x g for 5 min at 4°C, and the spent media was discarded. The cell pellet was resuspended in 50 mL yeast minimal expression media SG-CAA + 2% dextrose (20g/L galactose, 0.2 g/L dextrose, 6.7 g/L yeast nitrogen base, 5.0 g/L casamino acids, 10.4 g/L sodium citrate, 7.4 g/L citric acid monohydrate, pH 4.5) and allowed to incubate at 30°C while shaking at 230 rpm until the appropriate time point was reached.

2.2.3 Plasmid Construction

Plasmids containing the yeast surface display fusion protein were constructed using the pCTcon2-scFv-F4 plasmid [69], which is shown in Figure 2.2. This plasmid possesses a divergent galactose inducible promoter (GAL1,10) for the controlled expression of the surface display fusion. Additionally, pCTcon2-scFv-F4 incorporates an ampicillin resistance gene (AmpR) for easy viability selection during recombinant cloning and a phosphoribosylanthranilate isomerase gene for tryptophan biosynthesis (TRP1) for viability selection in tryptophan-deficient media. All peptides were genetically incorporated into the fusion protein using the primers provided in Table 2.2.

For the DNA encoding histatin 5, the primer pair NheI-Hst5-Top1 and Nhe-Hst5-Bot1 and the primer pair BamHI-Hst5-Top2 and BamHI-Hst5-Bot2 were 5' phosphorylated and annealed to create Hst5(1) and Hst5(2) respectively. The annealed Hst5(1) had a 5' NheI sticky end and the annealed Hst5(2) had a 3' BamHI sticky end; Hst5(1) and Hst5(2) had complementary sticky ends as well, allowing them to anneal together. The two primer pairs were inserted into pCTcon2 between

the NheI and BamHI cut sites to replace the DNA encoding scFv F4 in the source plasmid and generate pCTcon2-Hst5. Similarly, for the DNA encoding K11RK17R, the primer pair NheI-K11R-Top1 and NheI-K11R-Bot1 and the primer pair BamHI-K17R-Top1 and BamHI-K17R-Bot1 were 5' phosphorylated and annealed to create K11R(1) and K17R(2) respectively. The annealed K11R(1) had a 5' NheI sticky end and the annealed K17R(2) had a 3' BamHI sticky end; K11R(1) and K17R(2) had complementary sticky ends as well, allowing them to anneal together. The two pairs were inserted into pCTcon2 between the NheI and BamHI cut sites to replace the DNA encoding scFv F4 in the source plasmid and generate pCTcon2-K11RK17R. Similarly, for the DNA encoding K13L, the primer pair NheI-K13L-Top1 and NheI-K13L-Bot1 and the primer pair BamHI-Hst5-Top1 and BamHI-Hst5-Bot1 were 5' phosphorylated and annealed to create K13L(1) and Hst5(2) respectively. The annealed K13L(1) had a 5' NheI sticky end and the annealed Hst5(2) had a 3' BamHI sticky end; K11R(1) and K17R(2) had complementary sticky ends as well, allowing them to anneal together. The two pairs were inserted into pCTcon2 between the NheI and BamHI cut sites to replace the DNA encoding scFv-F4 in the source plasmid and generate pCTcon2-K13L.

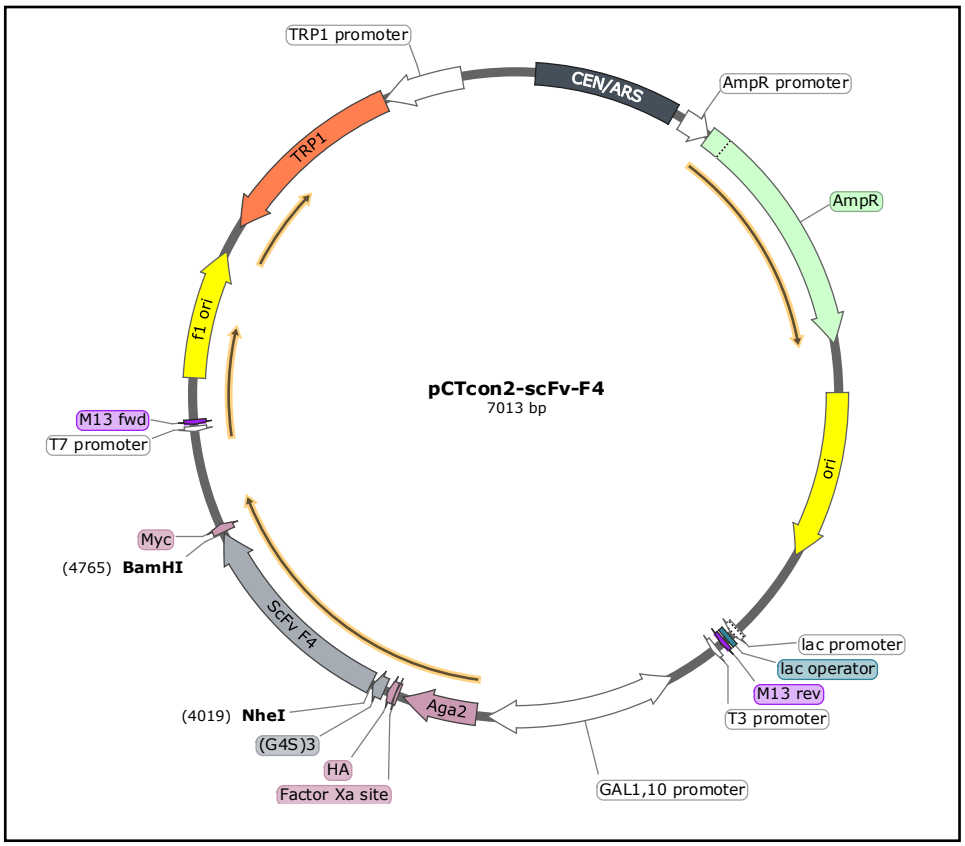

Figure 2.2: Illustration of pCTcon2-scFv-F4. Figure obtained from reference [69]. Expression of TRP1 and AmpR genes are regulated by the TRP1 and AmpR promoters, respectively. Expression of the yeast surface display fusion protein (Aga2-HA-POI-Myc) is regulated by the GAL1, 10 promoter. In this plasmid, the POI is the scFv-F4, which is flanked on either side by the restriction enzyme sites NheI and BamHI for easy substitution.

Table 2.2: Primers Used for Construction of pCTcon2 Plasmids

Primer Name	Sequence (5' to 3')
NheI-Hst5-Top1	CTAGCGATTCTCATGCAAAACGCCATCACGGGTATAAGCGCAAG
BamHI-Hst5-Top2	TTCCACGAAAAGCACCACAGTCATCGCGGGTACG
NheI-Hst5-Bot1	GAACTTGCGCTTATACCCGTGATGGCGTTTTGCATGAGAATCG
BamHI-Hst5-Bot2	GATCCGTACCCGCGATGACTGTGGTGCTTTTCGTG
NheI-K11R-Top1	CTAGCGATTCCCACGCGAAGCGTCATCATGGGTATCGTCGTAAG
NheI-K11R-Bot1	GAACTTACGACGATACCCATGATGACGCTTCGCGTGGGAATCG
BamHI-K17R-Top2	TTCCACGAGAGGCATCACAGTCATCGTGGATACG
BamHI-K17R-Bot2	GATCCGTATCCACGATGACTGTGATGCCTCTCGTG
NheI-K13L-Top1	CTAGCGATTCTCACGCAAAGCGTCATCACGGGTATAAAAGATTG
NheI-K13L-Bot1	GAACAATCTTTTATACCCGTGATGACGCTTTGCGTGAGAATCG
Forward-Seq-pCTcon2	GTTCCAGACTACGCTCTGCAGG
Reverse-Seq-pCTcon2	GATTTTGTTACATCTACACTGTTG

All plasmids were Sanger sequenced using the primers Forward-Seq-pCTcon2 and Reverse-Seq-pCTcon2 to confirm the correct construction of each construct. All plasmids were chemically transformed into *S. cerevisiae* strain EBY100 using the EZ Yeast Transformation II Kit (Zymo Research).

2.2.4 Western Blotting

Western blotting was performed by first harvesting a 50 mL expression culture of EBY100 cells transformed with the appropriate plasmids after 22 hours of incubation at 30°C while shaking at 230 rpm. Cells were initially centrifuged at 3,000 x g for 5 min at 4°C and the liquid was discarded. The cell pellet was resuspended in yeast protein extraction reagent (Y-PER, Thermo Scientific) to a concentration of 385 mg/mL and mixed on a microplate shaker (VWR) at 250 rpm for 20 min at room temperature. The cell solution was centrifuged at 14,000 x g for 10 min and the liquid portion was decanted as the "soluble protein fraction." The remaining cell pellet was resuspended in 150 µl of 8 M urea and was mixed for 20 min at room temperature prior to centrifugation at 11,000 x g for 15 min. The supernatant was decanted as the "insoluble protein fraction."

The fractions were adjusted to approximately equal protein concentrations, and each fraction was were mixed in 1:1 proportion with a 2X SDS+β-mercaptoethanol solution (95% (v/v) 2X SDS loading dye, 5% (v/v) β-mercaptoethanol) and were boiled at 98°C for 5 min before being loaded onto and run on a mini-PROTEIN® TGX precast gel (Bio-Rad) for 25 min at 200 V. The separated protein was transferred onto an Immobilon® transfer membrane (Millipore)

using the Trans-Blot® Turbo Transfer System (Bio-Rad) at 1 A, 25 V for 30 min. After transfer, the membrane was blocked with 5% (w/v) nonfat dry milk in Tris-buffered saline with Tween (TBST) (2.4 g/L Tris-HCl, 0.56 g/L Tris-base, 8.8g/L NaCl, 0.1% (v/v) Tween-20) for 1 h at room temperature and 230 rpm. The membrane was washed twice for 10 min with TBST and was incubated with the appropriate antibodies for 1 h to detect the epitope tags. The HA tag was detected with the primary anti-HA tag antibody (ab130275, Abcam) at 1:1,000 dilution in TBST followed by secondary rabbit anti-mouse IgG H+L antibody (HRP) (ab6728, Abcam) at 1:5,000 dilution in TBST. The C-Myc tag was detected with the anti-Myc tag antibody (HRP) (ab1326, Abcam) at 1:5,000 in TBST dilution. Six washes with TBST were performed between primary and secondary antibodies for HA detection. Both membranes were washed three times with TBST after labelling with HRP conjugated antibodies followed by one wash with Tris-buffer saline (TBS) (2.4 g/L Tris-HCl, 0.56 g/L Tris-base, 8.8g/L NaCl, pH 7.6). Clarity Western ECL Substrate (Bio-Rad) was used as the substrate for HRP, and membranes were imaged using a ChemiDoc MP imaging system (Bio-Rad).

2.2.5 Secreted Aspartic Proteases (Saps)

The secreted aspartic proteases (Saps) 2 and 9 were provided by Dr. Bernhard Hube from Friedrich Schiller University, Germany. The Saps were expressed in *Pichia pastoris* [70], and Sap9 was expressed without its GPI anchor [71].

2.2.6 Degradation of Expressed Fusion Peptides

After expression, the OD_{600} of the cell culture was measured and 4 x 10^6 cells were aliquoted and placed on ice. Cells were centrifuged at 16,000 x g for 1 min and liquid was removed. Cell pellets were washed three times with 1 mM sodium phosphate buffer (NaPB) (0.155 g/L $NaH_2PO_4 \bullet 7\ H_2O$, 0.058 g/L $Na_2HPO_4 \bullet H_2O$, pH 7.0) for degradation by Sap2 or Sap9. Cells were resuspended in 0.1 mL of 1 mM NaPB, Saps were added to the desired concentration, and samples were placed at 30°C on a microcentrifuge tube rotator (VWR) to avoid cell precipitation. As a control, a separate aliquot of cells was washed three times with ice-cold PBS (8 g/L NaCl, 0.2 g/L KCL, 1.44 g/L Na_2HPO_4, 0.24 g/L KH_2PO_4, pH 7.4) and was immediately labelled with antibodies for flow cytometry or fluorescent-activated cell sorting (FACS) analysis.

2.2.7 Preparation for Flow Cytometry and FACS

After incubation, cells were centrifuged at 16,000 × g for 1 min and the liquid was discarded. Cell pellets were washed three times with ice-cold PBS and were resuspended in 0.1 mL ice-cold PBS. Approximately 5 x 10^5 cells were retained for viability assessment. Primary antibodies anti-HA tag (ab130275, Abcam) and chicken anti-c-Myc epitope tag (ACMYC, Gallus) were added in 1:200 dilution and cells were incubated at 4°C on a microcentrifuge tube rotator for 30 min. Cells were centrifuged at 16,000 x g for 1 min, and liquid was discarded. The cell pellet was washed three times with ice-cold PBS and was resuspended in 0.1 mL ice-cold PBS. Secondary antibodies Alexa Flour 488 goat anti-mouse IgG H+L (A11029, Life Technologies) and Alexa Flour 647 goat anti-chicken IgG H+L (A21449, Life

Technologies) were added in 1:50 dilution, and cells were incubated at 4°C on the microcentrifuge tube rotator for 45 min while wrapped in foil to avoid light exposure. Cells were centrifuged at 16,000 x g for 1 min in minimal lighting and liquid was discarded. Cell pellets were washed three times with ice-cold PBS and were resuspended to 5 x 10^5 cells/mL in ice-cold PBS for flow cytometry or FACS analysis.

2.2.8 Sap Degradation Analysis

Degradation was assessed with flow cytometry (BD FACSCanto II), and data was analyzed using FlowJo software. For the analysis, an unlabeled cell control was used to establish the gating scheme for the samples analyzed in a given set of experiments. Gating of the cell control involved first isolating events measured during homogenous flow through the detector, followed by the isolation of single, live cells using the forward and side scatter filters. Events were plotted on a bivariate log-log plot of signals with Alexa-Flour 488 (corresponding to the labeling of the HA epitope tag) and APC (corresponding to the labeling of the C-Myc epitope tag) filters and quadrants were drawn to gate the entirety of the cell control in Q4. An identical gating scheme was applied to all related samples. The percent of events and both the means and standard deviations of both signals in each quadrant were recorded and used for statistical analysis (GraphPad Prism 8.01).

2.2.9 Cell Viability Analysis

Viability was assessed after incubation with Saps to evaluate the influence of different incubation conditions on the relative viable population size. An aliquot of 5

x 10^5 cells was diluted in PBS to a final concentration of 2.5 x 10^3 cell/mL, and 40 µl was spread on three YPD agar (10 g/L yeast extract, 20 g/L peptone, 20 g/L glucose, 2% (w/v) agar) plates. The plates were incubated at 30°C for 48 hours, and colonies were counted to determine the colony forming units (CFU) per mL for a given sample (n=3).

2.3 Results

2.3.1 Scope of Research

The incorporation of histatin 5, K11RK17R, and K13L into yeast surface display was performed to assess the utility of this system to screen for variants with enhanced proteolytic stability in the presence of Sap2 and Sap9. The role of pH, protease concentration, temperature, and time on the degradation of histatin 5 were investigated to identify optimal degradation conditions to be used for the interrogation of a future peptide library designed from histatin 5.

2.3.2 Validation of Fusion Expression by Western Blotting

Western blotting was performed to validate the expression of the full yeast surface display fusion protein generated by pCTcon2-Hst5 and the original plasmid pCTcon2-scFv-F4 in both soluble and insoluble protein fractions (Figure 2.3). Validation was performed by blotting for both HA and C-Myc epitope tags in both fractions with EBY100 cells not containing a transformed plasmid as a control.

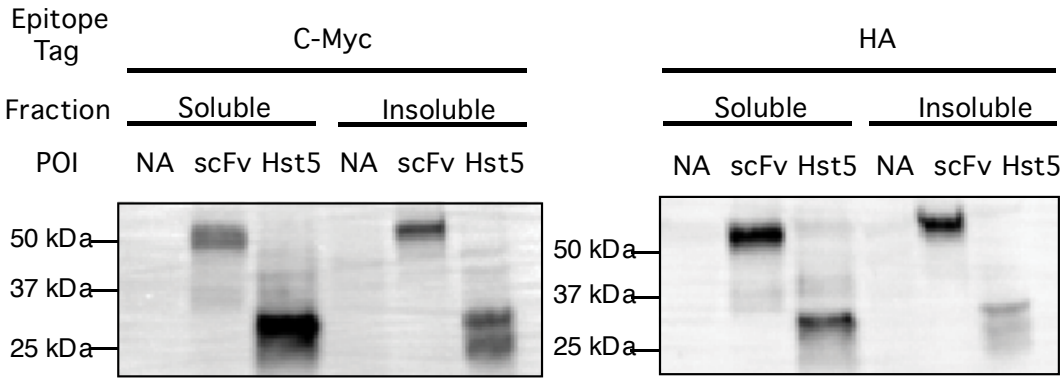

Figure 2.3: Western Blot of Aga2-Histatin 5 and Aga2-scFv-F4 Using pCTcon2 Plasmid. Detection of M-Myc and HA epitope tags are shown with the standard protein sizes determined from molecular weight ladder. EBY100 cells without either plasmid was run as a control along with fractions for Aga2-ScFv-F4 (scFv) and Aga2-histatin 5 (Hst5). The expected weights of Aga2-scFv-F4 and Aga2-Hst5 were approximately 42.7 kDa and 17.5 kDa, respectively.

Bands were observed for Aga2-scFv-F4 and Aga2-histatin 5 at approximately 53 kDa and 35 kDa, respectively for both C-Myc and HA epitope tag detection. While both bands are slightly larger in molecular weight than their expected band sizes, the displacement is uniform and is not uncommon to observe in Western blotting. The presence of a second degradation product band was also observed in the insoluble fraction of Aga2-histatin 5, which is occasionally observed in Western blotting. This validated the expression of the entire fusion in both cases as the presence of both epitope tags were detectable in the same band corresponding to the size of the whole protein fusion.

2.3.3 Optimizing Expression of Yeast Surface Display Fusion Protein

Expression optimization was initially performed with the plasmid pCTcon2-Hst5 and validated by flow cytometry to validate the expression of the fusion in each

cell while only labeling for the C-Myc epitope tag, indicating the presence of the full protein fusion. The goal was to determine the optimal conditions required to obtain the highest number of fusion proteins expressed per cell, ensuring easy interrogation of the expressed fusion protein in later proteolytic degradation assays. Expression was performed at both 30°C, which was recommended by the Boder and Wittrup [60], and 20°C, which was shown to be the optimal conditions for total mammalian protein expression *in S. cerevisiae* [72], for 6, 10, 14, 18, 22, and 26 h. For all samples, 4 x 10^6 cells were aliquoted and only labelled with an anti-c-Myc antibody, which would indicate the presence rest of the entire fusion construct. Cells expressing the full fusion were identified using a Myc+/Myc- gate calibrated from an unlabeled cell control and are shown in Figure 2.4.

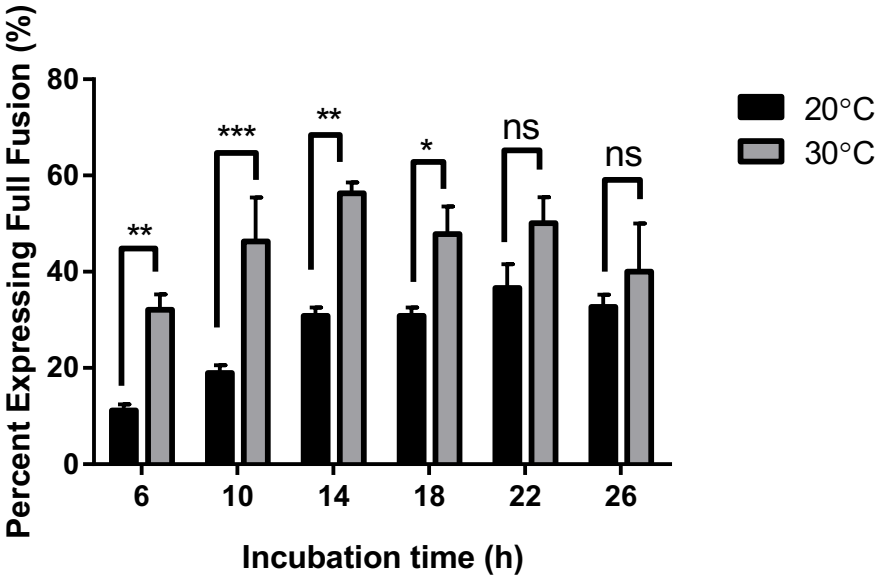

Figure 2.4: Fusion Protein Expression as a Function of Time and Temperature. All presented data correspond to the average of the percent of positively expressing cells based on two independent biological replicates (n=2) with error bars representing the standard deviation in the population. Expression of full construct was quantified by flow cytometry with an Alexa-Flour 647 goat antibody to detect the displayed construct. The number of asterisks indicates the level of significance: * for P<0.1, ** for P<0.01, and *** for P<0.001; ns indicates not significant).

Significantly higher levels of fusion expression per 4 x 10^6 cells were observed at 30°C compared to 20°C for all time points with the exception of 22 and 26 h. No significant difference was observed between all expressions performed at 30°C. Therefore, expression was conducted for 14 – 16 h for all future assays due to the high levels of accomplished expression and convenience.

2.3.4 Initial Degradation Profiles of Displayed Peptides

Prior to using yeast surface display to generate and screen a library of variants for improved proteolytic stability, initial degradation profiles were gathered to assess how distinguishable protease resistant (K11RK17R) and proteases susceptible (K13L) variants would be without optimization of degradation conditions. Therefore, an initial incubation of both variants displayed on the surface of yeast cells was performed for 2 h at 30°C with 200 μg/mL of both Sap2 and Sap9 with 4 x 10^6 cells in 1 mM NaPB. Flow cytometric analysis was performed on the resulting samples with antibody labelling of both HA and C-Myc epitope tags (Figure 2.5).

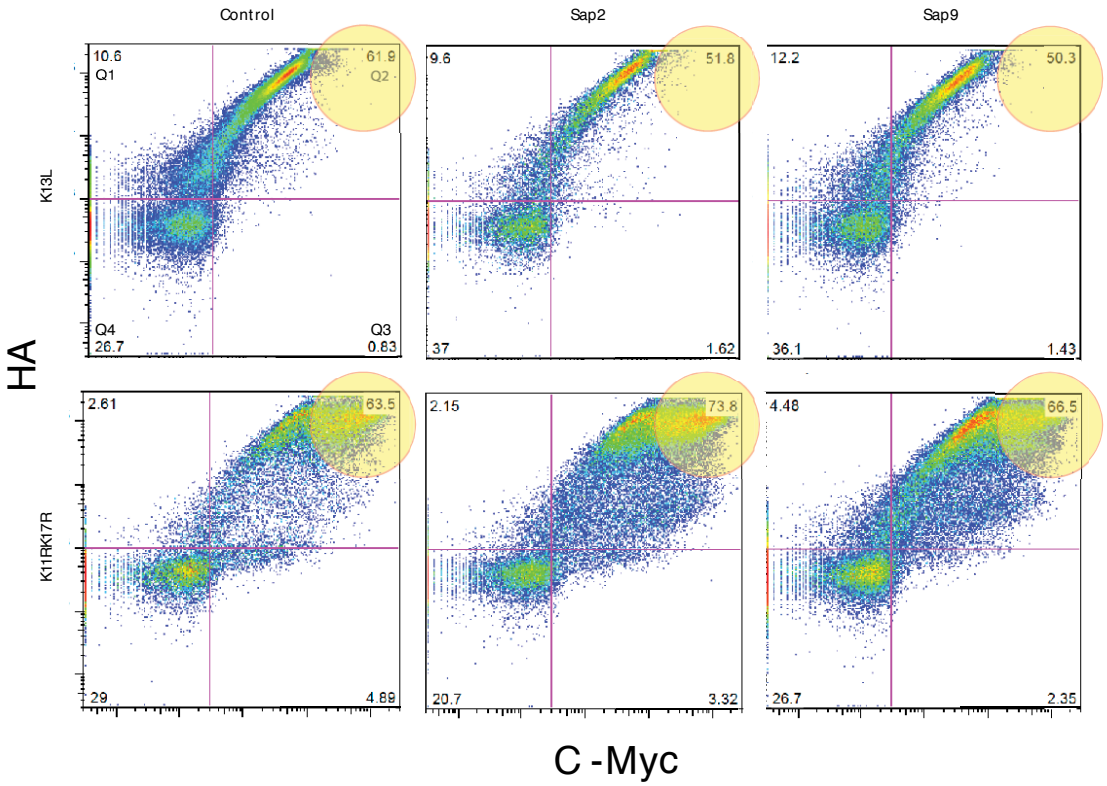

Figure 2.5: Initial Degradation Profiles of K11RK17R and K13L. Bivariate plots of the intensity for both HA (Alexa-Flour 488 antibody) and C-Myc (Alexa-Flour 647 antibody) were plotted with quadrants based on cell standards for both plasmids. Each dot corresponds to a single cell and density of cells is indicated by heat map. Numbers located in the corner of each quadrant represent the percent of total events located within each boundary. Yellow circles included to highlight region of focus for variants with high proteolytic stability.

As expected, high levels of degradation were observed in the less stable variant, K13L, compared to K11RK17R, which is indicated by a lower mean intensity of C-Myc in Q2 (HA+/C-Myc+) in the presence of Sap2 and Sap9 (Table 2.3). Additionally, a more drastic left-ward shift is present for K13L, resulting in a higher percentage of events in the Q1 (HA+/C-Myc-). Therefore, the proteolytic stability properties of both peptides are conserved in the yeast surface display fusion and agree with prior degradation findings observed with purified peptide [53]. A high activity of Sap9 for both substrates is also present in the comparison of degradation profiles

between Sap9 and Sap2 indicated by a proportion of cells within Q1, which is in-line with prior findings [53].

Table 2.3: Raw Preliminary Degradation Profile Data for Quadrants Q1 and Q2

Peptide	Sap	Q1 (HA+/Myc-)*		Q2 (HA+/Myc+)*	
		HA	C-Myc	HA	C-Myc
K11RK17R	NA	2618 ± 1833	149 ± 83.8	83904 ± 60119	31919 ± 38892
	2	2653 ± 1975	144 ± 85.8	81078 ± 58748	32579 ± 39243
	9	2788 ± 2018	143 ± 85.2	75025 ± 63224	22621 ± 32029
K13L	NA	3247 ± 2403	133 ± 84.7	81110 ± 56314	3979 ± 3993
	2	3413 ± 2807	141 ± 84	86589 ± 68916	4339 ± 5401
	9	3255 ± 2580	138 ± 83.9	68542 ± 55095	3170 ± 3333

*Values represent the average of three biological replicates ± the standard deviation in the population (n=3).

While these findings did agree with initial expectations, a larger contrast between variants with high and low proteolytic stability was desired for the enrichment of novel variants with superior stability. Therefore, optimization of the degradation conditions was performed to increase the contrast between K11RK17R and K13L.

2.3.5 pH Optimization of Proteolytic Degradation

As a first round of optimization, the role of pH was investigated on the activity of both Sap2 and Sap9 to degrade K11RK17R and K13L. A literature search found that the optimal conditions for Sap2 activity were commonly observed at pH 3.5 – 4.0 and pH 5.0 – 5.5 for Sap9 in low salt sodium citrate or acetate buffer (Table 2.4).

Table 2.4: Reported Conditions for Optimum Activity of Saps 2 and 9

Sap	Reported Optimum pH	Buffer Conditions	Source
2	4.0	100 mM citric acid	[52]
2	4.0	10 mM acetate	[73]
2	3.5	50 mM Na citrate	[70]
2	4.0	50 mM Na citrate	[51]
2	3.2-3.5	50 mM Na citrate	[49]
9	5.0	10 mM acetate	[73]
9	5.5	50 mM Na citrate	[51]

Due to the more common usage of citrate buffer over acetate or sodium phosphate buffer, the degradation of both Saps at new conditions of pH 4.0 in 10 mM sodium citrate for Sap2 and pH 5.0 in 10 mM sodium citrate for Sap9 was conducted. The resolution of these degradation profiles was compared to those obtained with the original conditions of 1mM NaPB. Degradation for both Saps was performed on K11RK17R and K13L for 2 h at 30°C in both the original and new conditions and the analysis was performed by flow cytometry with gating for the positive C-Myc signal, which would indicate the presence of the full fusion (Figure 2.6).

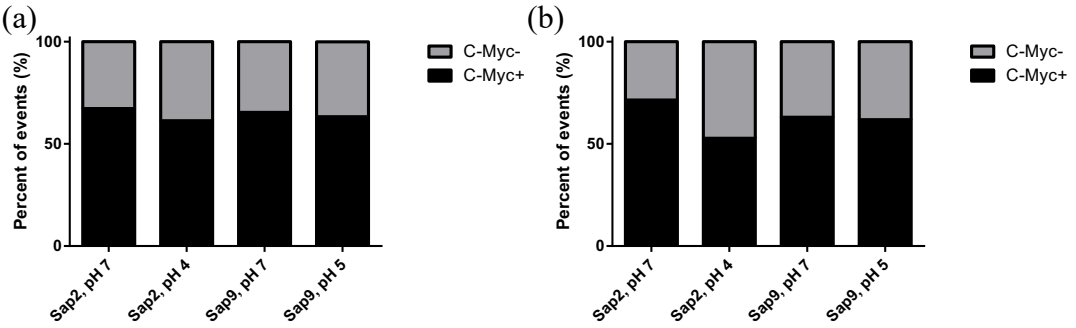

Figure 2.6: Influence of pH on Degraded with Sap2 and Sap9. K11RK17R (a) and K13L (b) are displayed with C-Myc (Alexa-Flour 647 antibody) positive, corresponding to the presence of the full fusion protein, and C-Myc negative, corresponding to degraded fusion protein, proportions for a single biological replicate (n=1). Degradation at pH 4 and 5 was performed in 10 mM citrate buffer and degradation at pH 7 was performed in 1 mM NaPB.

Degradation at lower pH resulted in a small increase in the degradation of both K11RK17R and K13L, which is observed by comparing the percentage of events gated for positive C-Myc signal (Figure 2.6). Comparing the mean C-Myc signal in the positively expressing cells showed a decrease in the C-Myc signal for K11RK17R for both Sap2 and Sap9 with similar variability in populations at reduced pH, indicating that 10 mM citrate buffer encouraged enhanced degradation (Supp. Table A.1). The opposite trend, with decreasing pH resulting in an increased mean C-Myc signal, was observed for K13L with both Sap2 and Sap9. However, the standard deviation of K13L positively expressing the fusion was doubled in 10 mM citrate buffer, indicating that the observed decrease in degradation was due to a more heterogeneous treatment of each yeast cell. Comparing the pH of the degradation conditions before and after incubation demonstrated that sodium citrate did a better job of maintaining the pH than the NaPB did. Therefore, 10 mM citrate buffer at pH 4 or 5 for Sap 2 and Sap9, respectively, were accepted for later optimization experiments for better maintenance of degradation conditions.

2.3.6 Scale Down Analysis

In anticipation of the large number of samples and reagent resources required to optimize for temperature and time of incubation, investigation into scaling down the degradation conditions was performed. This was examined at the previously used Sap concentration (200 μg/L) with both 4 x 10^6 cells and a reduced cell count of 2 x 10^6. To also see if increasing the concentration of Saps could significantly increase the degradation, a higher concentration of Saps was analyzed in parallel (1000 μg/mL). This round of experiments was performed on the histatin 5 fusion with only

Sap2 due to its inferior degradation of both K11RK17R and K13L compared to Sap9 in the preliminary degradation study (Figure 2.7). All degradation experiments were performed in 10 mM citrate buffer at pH 4.0 for 2 h at 30°C. Analysis was performed by comparing the percent of events in both quadrants Q1 (HA+/Myc-) and Q2 (HA+/Myc+) resulting from either incubation condition.

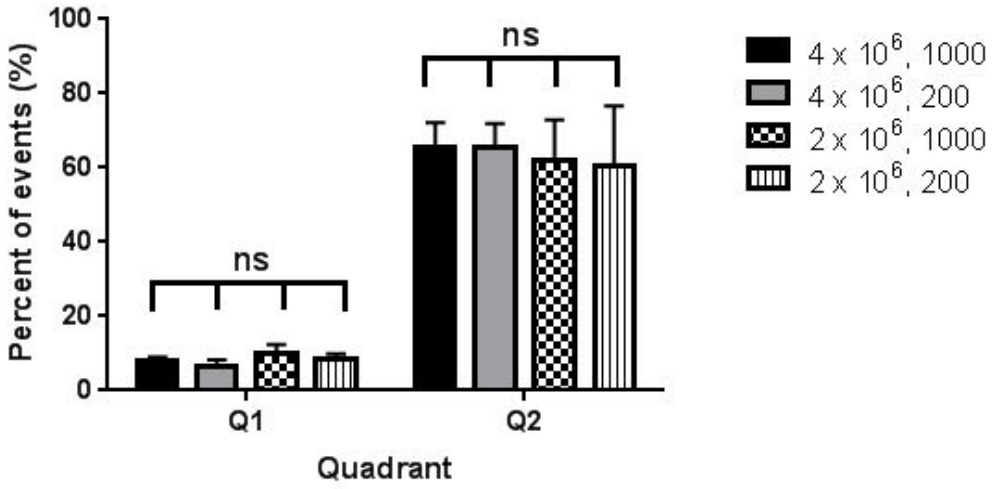

Figure 2.7: Degradation of Histatin 5 with High and Normal Sap2 Proportions. All presented data corresponds to the average of three independent biological replicates (n=3) with error bars indicating the standard deviation of the populations. Data labels on the x-axis correspond to the observed quadrants with Q1 (HA+/Myc-) indicating cells with positive HA (Alexa-Flour 488 antibody) signal and negative C-Myc (Alexa-Flour 647 antibody) signal and Q2 (HA+/Myc+) indicating cells with positive HA and C-Myc signals. Legend denotes populations of "cell count, Sap2 concentration in μg/mL." No significant difference was identified in the comparison between all pairs of conditions.

Neither scaling down the number of cells nor increasing the amount of present Sap2 resulted in an increase in the degradation of histatin 5 (Figure 2.7). However, a significant decrease in the mean C-Myc signal from 8149 ± 21876 to 4462 ± 14168 in Q2 was observed between 4 x 10^6 cells with 200 μg/mL of Sap2 and 2 x 10^6 cells with 1000 μg/mL of Sap2 (Supp. Table A.2). Therefore, significant partial

degradation of the fusion is achieved by increasing the ratio of Sap2 to cells. Therefore, future degradation optimization was performed at 2 x 10^6 cells with 1000 μg/mL of Saps to encourage efficacious interrogation of the expressed fusion protein.

To verify that neither the addition of Saps nor the incubation conditions significantly reduced the number of viable cells, viability analysis was also performed. Cell viability is important in this case as only live cells can be isolated and replicated from a peptide library. Therefore, it is important to avoid conditions that significantly reduce the number of variants that can be screened to preserve the size of a given peptide library.

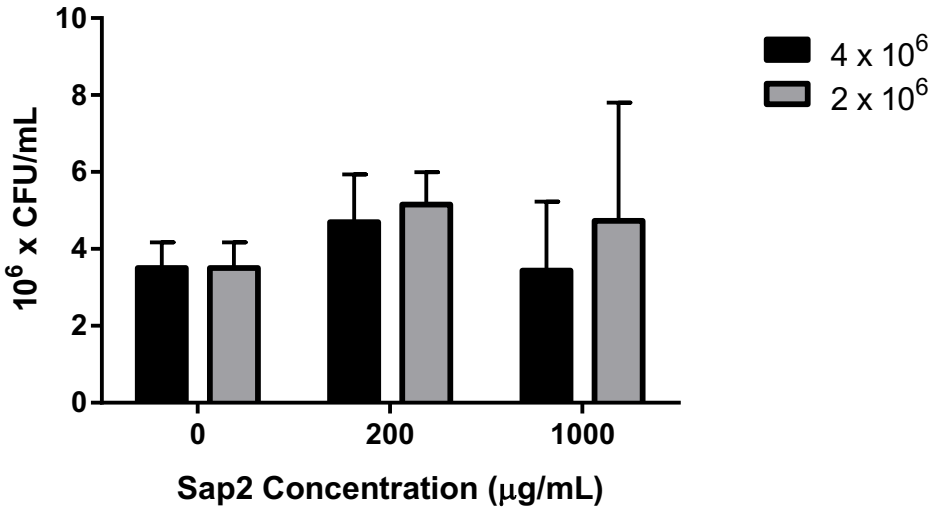

Figure 2.8: Viability Analysis of Scale-Down Conditions. All presented data corresponds to the average of three independent biological replicates (n=3) measured by a single measurement with error bars indicating the standard deviation of the populations. Data labels in the legend correspond to the number of cells in either condition. No significant difference was identified in the comparison between all pairs of conditions.

No significant influence of degradation conditions or Sap2 proportions was observed on the cellular viability (Figure 2.8). Therefore, reducing the cell amount

and increasing the Sap2 concentration can be used without significantly reducing the library size. While each condition exhibited a large variance, this was attributed to the lack of replicate measurements taken for each biologically independent sample. This was addressed in later experiments by taking triplicate measurements within a sample at each condition for viability analysis.

2.3.7 Optimization of Time and Temperature

The influence of both time and temperature on the degradation of the histatin 5 fusion was performed in parallel to identify optimal conditions for degradation. To examine the influence of these parameters, a cell count of 2 x 10^6 and a Sap2 concentration of 1000 μg/mL was used at 30°C and 37°C for durations of 2, 4, and 6 h. This analysis was performed using flow cytometry and by comparing the resulting proportions of events in quadrants Q1, corresponding to degraded peptide, and Q2, corresponding to intact peptide.

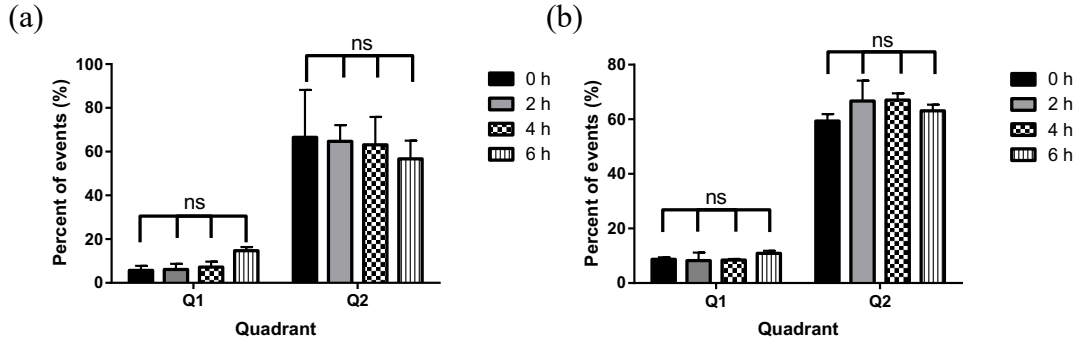

Figure 2.9: Degradation of Histatin 5 as a Function of Time and Temperature. Degradation performed at 30°C (a) and 37°C (b) are presented. All presented data corresponds to the average of three independent biological replicates (n=3) with error bars indicating the standard deviation of the populations. Data labels in the legend correspond to the observed quadrants with Q2 (HA+/Myc+) indicating cells with positive HA (Alexa-Flour 488 antibody) and C-Myc (Alexa-Flour 647 antibody) signals and Q1 (HA+/Myc-) indicating cells with positive HA signal and negative C-Myc signal. Time was not found to have a significant influence on the Q1 (HA+/Myc-) or Q2 (HA+/Myc+) proportions at either temperature (ns).

Comparison of the proportions present in either quadrant of interest did not yield a significant increase in degradation of histatin 5 with increasing time of incubation at 30°C and 37°C (Figure 2.9). The same was also observed for the influence of temperature on the degradation of histatin 5 at all observed time points (Figure 2.10). However, a decrease in the mean C-Myc signal in Q2 was observed with increasing time of incubation from 4323 ± 13611 at the original conditions of 2 h and 30°C to 2136 ± 12012 and 2877 ± 9159 at 6 h for 30°C and 37°C, respectively (Supp. Table A.3). Therefore, partial degradation of the expressed fusions per cell is primarily observed here as was observed in previous optimization experiments. Increasing the degradation of histatin 5 from 2 h to 6 h also resulted in a significant decrease in the variability of the C-Myc signal, indicating that more homogenous degradation was accomplished at longer incubation times. Therefore, degradation of histatin 5 for 6 h at 30°C was chosen as the time and temperature to perform subsequent experiments on the degradation of K11RK17R and K13L.

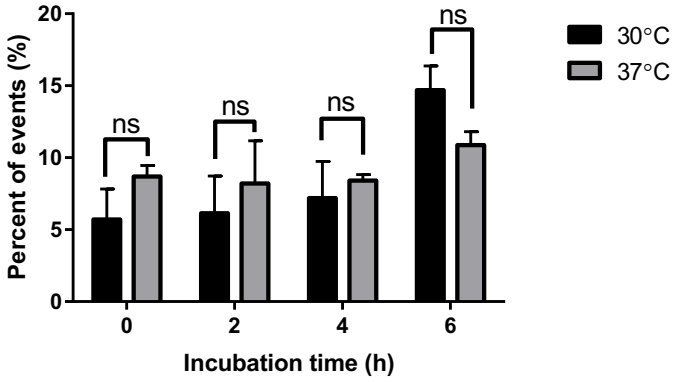

Figure 2.10: Influence of Temperature and Time on Histatin 5 Degradation. Data correspond to the average of Q1 (HA+/Myc-) events from three independent biological replicates (n=3) with error bars indicating the standard deviation of the populations. Data was obtained using flow cytometry. No statistical significance was observed between temperatures at each time point (ns).

The effect of the temperature and time on viability analysis was evaluated with triplicate measurements for each replicate to better capture the true variability in the cell count of each sample. No significant difference in the cell count was observed between incubation temperatures and times up to 6 h (Figure 2.11). Therefore, final degradation at 6 h and 30°C should not limit the size of the library that can be tested and can be used for the final degradation analysis.

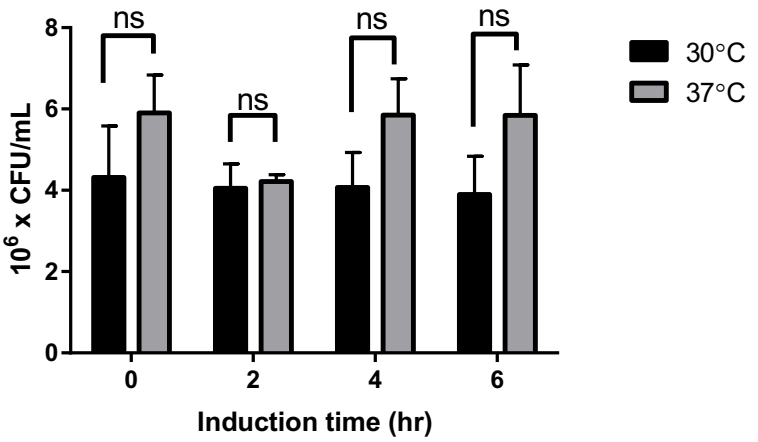

Figure 2.11: Viability Analysis for Optimization of Degradation Time and Temperature. All presented data corresponds to the average from three independent biological replicates (n=3) with error bars indicating the standard deviation of the populations. Triplicate measurements were taken for each biological replicate. No statistical significance was observed between cell count at any temperature or time (ns).

2.3.8 Degradation of K13L and K11RK17R

After optimizing the pH, proportion of cells to Saps, time, and temperature of the degradation conditions for histatin 5 with Sap2, degradation profiles were gathered for K11RK17R, K13L, and histatin 5 to re-assess the resolution between variants with variable proteolytic stability. Degradation was performed using the previously identified conditions of 2 x 10^6 cells with 1000 μg/mL of Sap2 or Sap9 at

30°C for 6 h in 10 mM citrate buffer at pH 4.0 for Sap2 and pH 5.0 for Sap9 were analyzed using flow cytometry (Figure 2.12).

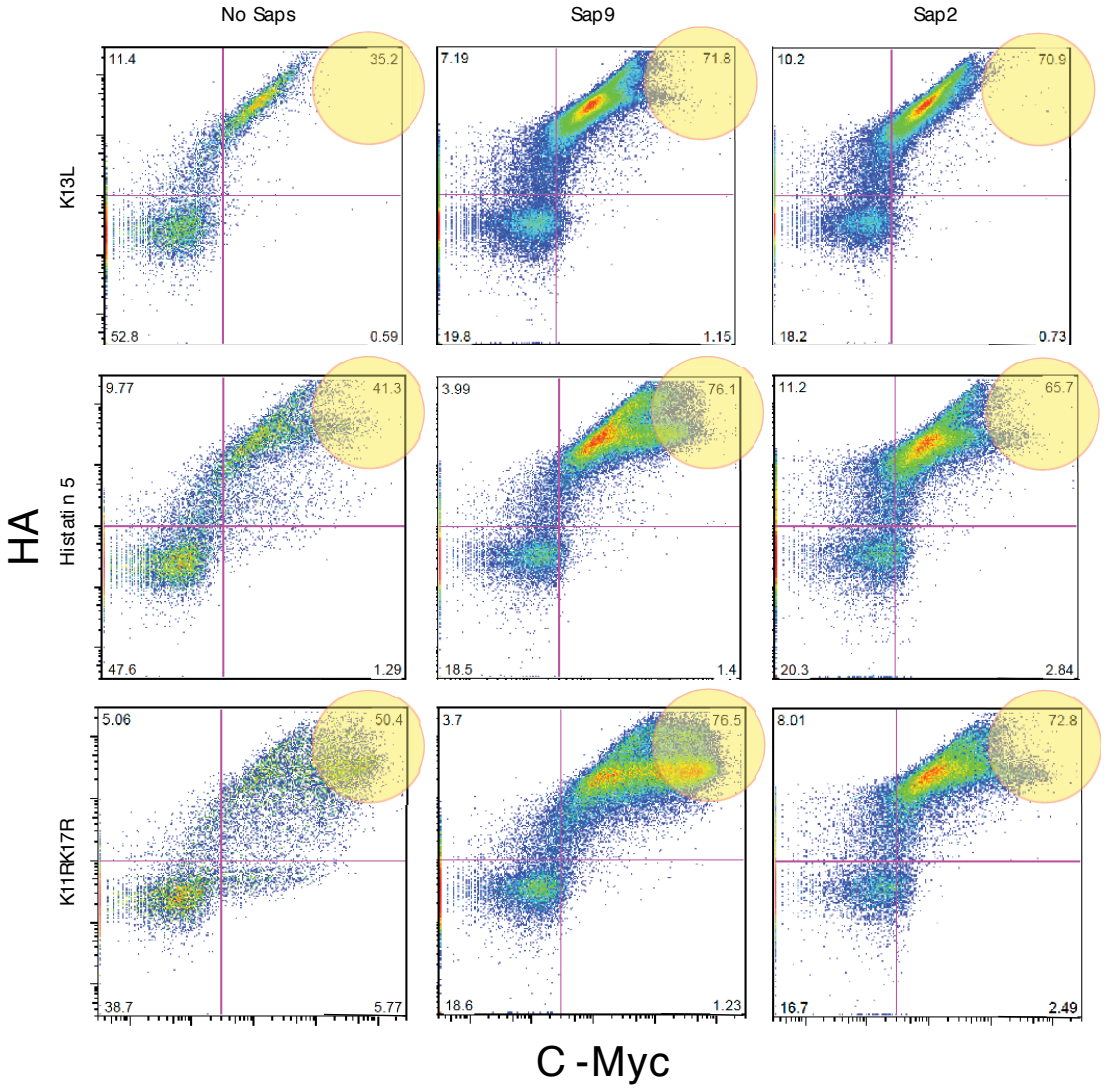

Figure 2.12: Degradation Profiles. Bivariate plots are plotted for degradation of histatin 5, K11RK17R, and K13L without Saps and with Sap2 and Sap9. The HA signal is produced by the Alexa-Flour 647 antibody while C-Myc is produced by the Alexa-Flour 488 antibody. Percent of events within each quadrant are displayed in each corner with Q1 pertaining to the top-left, Q2 for the top-right, Q3 for the bottom-right, and Q4 for the bottom-left. Each dot represents a single cell with the density of cells being plotted in as a heat map. Yellow circles included to highlight region of focus for variants with high proteolytic stability.

From the bivariate plots, a visible difference in the degradation profiles between K13L and K11RK17R is present after exposure to Saps. While events can

still be visible at high C-Myc signal for K11RK17R, there are almost no events present in this location for K13L after degradation with both Sap2 or Sap9. Therefore, isolating variants with high proteolytic stability over those with lower proteolytic stability should be possible at these degradation conditions. Compared to the original degradation conditions, an overall reduction in the C-Myc signal of cells expressed in Q2 is observed (Figure 2.12), indicating that higher levels of degradation are observed under optimal degradation conditions. A significant decrease in the variability of the C-Myc signal for K11RK17R degraded by Sap2 is also observed by performing degradation under the new optimum conditions (Figure 2.13). Therefore, a more homogenous degradation activity compared to that performed under the original degradation conditions can be obtained, improving the stringency of this yeast surface display system for the screening of variants with higher proteolytic stability.

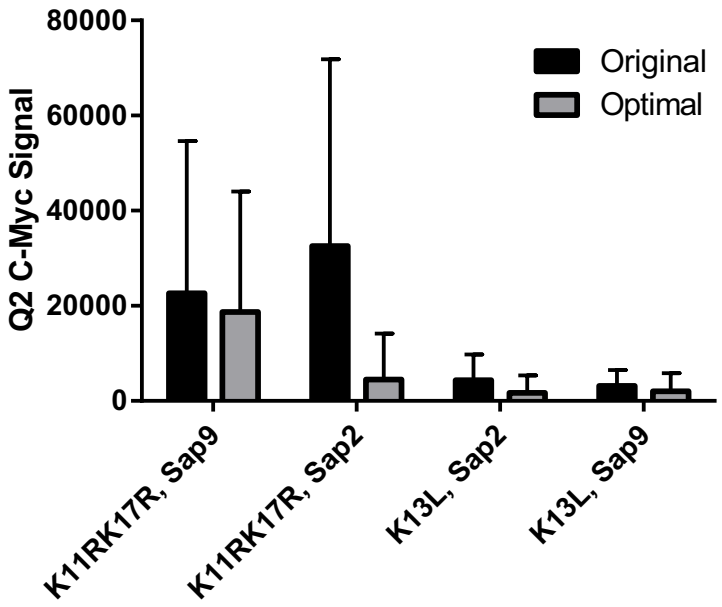

Figure 2.13: Comparison of C-Myc Signal in Positively Expressing Cells Before and After Optimization. All presented data corresponds to the average from one independent biological replicate (n=1) with error bars indicating the standard deviation of each sample. No statistical analysis was conducted to compare means since only one replicate was performed for both conditions.

The degradation behavior observed in the samples without Sap addition do not follow the same left-ward shift observed in the Sap9 and Sap2 samples (Figure 2.12). This is because these are incubated on ice for extended periods of time before being analyzed by flow cytometry in parallel with the Sap degraded samples, reducing the number of live cells that positively express the fusion. This is visible in the larger Q4 (HA-/Myc-) populations, which display no fusion protein. Therefore, the comparison in Q1 (HA+/Myc-) to Q2 (HA+/Myc+) populations between K11RK17R, histatin5, and K13L tell more about the stability of the peptide in solution with K11RK17R showing higher stability than histatin 5, which is higher than K13L.

2.4 Discussion

The peptides histatin 5, K11RK17R, and K13L were shown to be successfully integrated into the yeast surface display system with Western blotting. This ensures that other antifungal peptides can be easily integrated into this system as well for screening, which will be important for improving the fitness of the protein/peptide of interest. Furthermore, it was demonstrated in this chapter that histatin 5 as well as K11RK17R and K13L can be degraded by Saps while expressed in a fusion protein. This is valuable as it indicates that proteolytic stability can be assessed using this yeast surface display system. Therefore, histatin 5 can be engineered for improved proteolytic stability to Sap2 and Sap9 as well as other Saps or proteases of interest as needed.

Optimizing the degradation conditions of the yeast surface display containing the histatin 5 with Sap2 resulted in an increase in the degradation of all displayed fusion peptides. This observation was supported by comparison of the original degradation conditions in 1 mM NaPB at pH 7 with 200 μg/mL and 30°C for 2 h with the final conditions of 10 mM citrate buffer with 1000 μg/mL of Sap2 at pH 4.0 or Sap9 at pH 5.0 and 30°C for 6 h. Overall, an increase in the resolution between the degradation profiles of K11RK17R and K13L was observed, allowing for the isolation of variants with superior proteolytic stability when screening a library of peptides. Additionally, is it likely that several rounds of enrichment with FACS can ensure that sufficient segregation is accomplished between mutants with desired proteolytic stability and those without.

In general, while increased resolution was accomplished in this study, a higher degree of contrast is desired. Given that all viability assessments showed no significant difference between the conditions tested as a part of optimization, more stringent conditions could be tested in later experiments to increase the degradation pressure on the displayed peptides. This could be accomplished by increasing the incubation time with Saps beyond 6 h, to allow for more time for peptide interrogation by Saps, or by increasing the ratio of Saps to yeast cells, increasing the number of Saps present to interrogate the displayed peptides.

Chapter 3: Incorporating Antifungal Peptides into Polyelectrolyte Multilayer Films (PEMs)

3.1 Introduction

Adherence of *C. albicans* and maturation of biofilms on or within new medical devices introduced to the body, such as catheters [74, 75], wound dressings [74, 75], prosthetics [74], and orthopedic implants [75, 76], are both a financial and medical concern. Caused by fungal and bacterial pathogens, these hospital-acquired infections represent one of the most serious complications that can arise post-surgery or critical care [75]. Biofilms are responsible for approximately 64% of all bacterial and fungal hospital-acquired infections, and the prevention of these infections remains a key concern not only for those susceptible to candidiasis but bacterial infection as well [76]. In response to this, the application of polyelectrolyte multilayer films (PEMs) to the surfaces of medical devices represents a promising solution that can be used to mitigate both bacterial and fungal infections in vivo [75, 76].

PEMs consist of alternating layers of polycationic and polyanionic species that can be sequentially deposited onto a substrate of choice through layer-by-layer (LBL) deposition [77, 78]. LBL deposition involves the serial dipping of the substrate in premade polyelectrolyte and drug solutions, each followed by washing steps, to coat the coat the substrate surface in a multilayer film. An illustration of this process is shown in Figure 3.1 [77, 78].

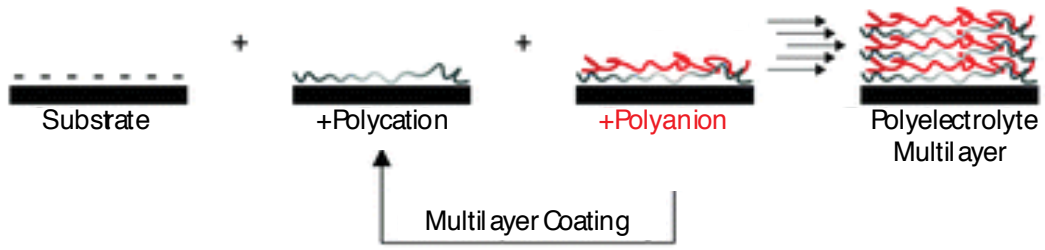

Figure 3.1: Illustration of PEM Film Generation by Layer-By-Layer (LBL) Deposition. Figure republished with permission of Royal Society of Chemistry, from [78]; permission conveyed through Copyright Clearance Center, Inc. LBL deposition is performed by serially soaking the negatively charged substrate surface with alternating solutions of polycation and polyanion to establish a polyelectrolyte multilayer film composed of repeating polycation/polyanion bilayers.

Additionally, PEMs can incorporate drugs that provide contact and slow-release antifungal and antibacterial action, reducing the risk of infection, which is illustrated in Figure 3.2 [75, 76, 77]. Therefore, PEMs can prevent the initial adherence and subsequent infection of bacterial and fungal pathogens.

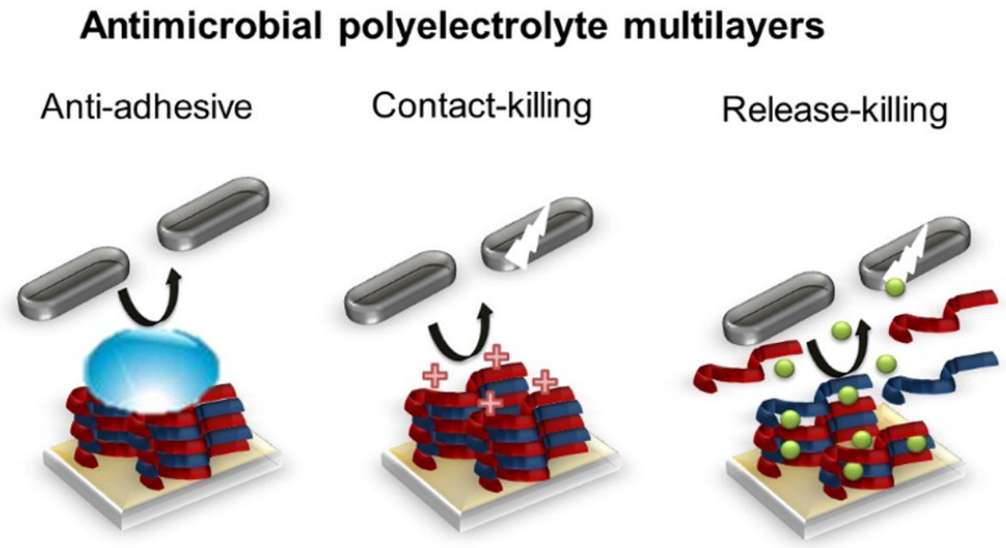

Figure 3.2: Illustration of the Antimicrobial/Antifungal Action of Drug-Loaded PEMs. Figure was reproduced from reference with permission from ACS [75]. Polyelectrolyte multilayer films prevent bacterial and fungal colonization by preventing initial adhesion, killing the pathogen upon contact with exposed drugs embedded in the PEM surface, and killing the pathogens in the surrounding environment as drug is slowly released over time.

PEMs can also be applied to a variety of substrates of various materials and geometries with highly tunable properties that are dependent on the polyelectrolytes used and the pH, ionic strength, and temperature of their solutions [75, 77, 79]. PEMs are also highly stable and can be stored under dehydrated conditions at ambient temperatures for extended periods of time until needed [78]. Given these beneficial properties, PEMs are highly versatile and may be engineered to prevent biofilm-associated *C. albicans* infections.

Studies have been conducted to determine this possibility of treating *C. albicans* with drug-incorporated PEMs. For example, β-peptides were incorporated into a poly(L-glutamic acid)/poly(L-lysine) (PGA/PLL) film using a dipping solution at a concentration of 1 mg/mL and exhibited significant antifungal activity against *C. albicans* [80]. The β-peptides in this instance were released into the surrounding solution for up to 400 hours, resulting in a 20% reduction in cell viability after 2 h and a 74% reduction in metabolic activity after 7 h [80]. Additionally, these same PEMs were coated onto catheter tubing and obtained similar results [81]. Chlorhexidine has also been incorporated into PEMs composed of poly(ethyl methacrylate)/tetrahydrofurfuryl methacrylate at the high dose of 16.5 mg per 10 mm disk and reduced biofilm development by 75% and reduced metabolic activity by 84% [82]. Given these examples, histatin 5 and the related antifungal peptide K11RK17R are promising for incorporation into PEMs to prevent infections.

3.2 Materials and Methods

3.2.1 Polyelectrolyte Multilayer Film (PEM) Fabrication

3.2.1.1 Peptides

The peptides used in this study (Table 3.1) were commercially synthesized (Genscript) with ≥95% purity and trifluoracetic acid salt removal by exchange to chloride. The lyophilized peptides were reconstituted in water and diluted in 20mM NaCl to the desired concentrations.

Table 3.1: Peptides Used for Polyelectrolyte Multilayer Films

Peptide	Sequence**	MW (Da)	Net Charge*
Histatin 5	D S H A K R H H G Y K R K F H E K H H S H R G Y	3036	+12
K11RK17R	- - - - - - - - - - R - - - - - R - - - - - - -	3092	+12

*Net charge (pH 7.0) is calculated only from the amino acid side chains and does not include charge from the N-terminal amine.
**Dashes indicate unchanged amino acids previously found in parent peptide.

3.2.1.2 Polyelectrolyte Multilayer Film (PEM) Fabrication

Silicon and quartz substrates were cut into 7 x 18 mm chips, serially cleaned with acetone, ethanol, methanol, and deionized water, and dried under a filtered air stream. Substrates were treated with oxygen plasma for 5 min using a 4000 Series Branson Barrel Resist Stripper (Branson International Plasma Corporation) to impart negative charge on the surface of the substrate. Base layers were deposited onto the substrate surface using polyethylenimine (PEI) and sulfonated polystyrene (SPS) solutions. A solution of 50 mM PEI (MW = 50,000, Sigma-Aldrich) was prepared in 25 mM NaCl and 5 mM HCl in water and was sterile filtered using a 0.22 μm filter before use. A solution of 50 mM SPS (MW = 70,000, Sigma-Aldrich) was prepared

in 25 mM NaCl in water and was sterile filtered using a 0.22 μm filter before use. PEI and SPS were deposited onto the treated substrate by (1) soaking the chip in the PEI solution for 5 min, (2) washing the chip twice by soaking in water for 1 min per wash, (3) soaking the chip in the SPS solution for 5 min, and (4) washing the chip twice by soaking in water as before. Steps (1) through (4) were repeated until 10 PEI/SPS bilayers were formed. The fabrication of these PEI/SPS base layers was performed on a DR3 dipping robot (Reigler & Kirstein GmbH). Following fabrication, the substrates were dried under a filtered air stream.

Peptides were deposited onto the base layers by incorporating a step of dipping into a peptide solution between dipping in the poly-L-glutamic acid and poly-L-lysine polymer solutions. Solutions of poly-L-glutamic acid sodium salt (PGA, MW = 50,000 – 100,000 for experiments with quartz and >50,000 for the experiments with silicon, Sigma-Aldrich) and poly-L-lysine hydrobromide (PLL, MW = 15,000 – 30,000, Sigma-Aldrich) were prepared at a concentration of 1 mg/ml in 20 mM NaCl in water. The peptides were diluted in 20 mM NaCl to either 1mg/ml or 3 mg/ml and the absorbance at 280 nm was measured prior to use. Films were fabricated by (1) soaking the chip in the PGA solution for 5 min, (2) washing the chip twice by soaking in water for 1 min per wash, (3) soaking the chip in the peptide solution with the desired concentration for 5 min, (4) washing the chip twice with water as before, (5) soaking the chip in the PLL solution for 5 min, and (6) washing the chip twice with water as before. Steps (1) through (6) were repeated until 60 trilayers (one trilayer consists of PGA-peptide-PLL) were formed. For control chips, water was used in place of the peptide solutions. The fabrication of these polyelectrolyte multilayer

films was performed on a DR3 dipping robot (Reigler & Kirstein GmbH). Following fabrication, the films were dried under a filtered air stream. The absorbance at 280 nm of the quartz chips as well as the solutions was measured after centrifuging at 15,000 xg for 5 min.

3.2.1.3 Thickness Characterization

Film thickness was characterized for silicon substrates post-fabrication. The measurements were performed by an LSE Model Gaertner Ellipsometer (Gaertner Scientific Corporation) with an incidence angle of 70°. Five measurements were taken along the center of each chip and were averaged to approximate the overall thickness of the film on the substrate.

3.2.2 Biofilm Inhibition Assays

3.2.2.1 Strains and Culture Conditions

The fungal pathogen *C. albicans* strain ATCC90028 was purchased from the American Type Culture Collection (ATCC). Cells were first inoculated from a yeast-peptone-dextrose (YPD) agar (10 g/L yeast extract, 20 g/L peptone, 20 g/L glucose, 2% (w/v) agar) plate into 8 mL of YPD liquid medium and grown overnight (≈16 h) at 30°C while shaking at 230 rpm. The overnight cell culture was subsequently subcultured into 25 mL of fresh liquid YPD at a starting OD_{600} of 0.1. The culture was grown at 30°C while shaking at 230 rpm until mid-log growth phase (≈3.5-4 h with an OD_{600} of ≈1.0). An aliquot of 10^7 cells was centrifuged at 2,000 rpm for 5 min and the liquid was discarded. The cell pellet was washed 3 times with PBS (8 g/L NaCl, 0.2 g/L KCl, 1.44 g/L Na_2HPO_4, 0.24 g/L KH_2PO_4, pH 7.4) and was

resuspended in 50% RPMI 1640 media (5.2 g/L RPMI 1640, 17.265 g/L MOPS, pH 7.0 ± 0.1) in water to 5 x 10^5 cells/mL.

3.2.2.2 *C. albicans* Seeding and Biofilm Formation

Chips coated using either 0, 1, or 3 mg/ml of either peptide in Table 3.1 were placed in individual wells of Nunc® Lab-Tek® II coverglass-bottomed, 4-well chamber slides. The *C. albicans* cell suspension was added to each well containing a chip, and 50% RPMI 1640 media (Gibco) was added to the remaining empty well as sterility control (500 µl/well). The chamber slide was sealed with parafilm and incubated at 37°C for 2 h to allow *C. albicans* to adhere to the film surfaces.

After 2 h, chips were transferred to a new chamber slide cassette after gently washing with PBS and fresh 50% RPMI 1640 media was added to each chip (500 µl/well). The entirety of the media control was transferred to an unoccupied well on the new cassette. The new cassette was sealed with parafilm and incubated at 37°C. Chamber slides were momentarily removed at 6, 12, and 18 h and finally removed at 24 h for microscopy analysis followed by growth inhibition characterization and a final round of microscopy.

3.2.2.3 Microscopy

Microscopy characterization of quartz chips was conducted using an Olympus IX83 microscope at 6, 12, 18, and 24 h after seeding. At each time point, a minimum of 3 images were taken at random locations over the top face of the substrate using a bright field (BF) filter using both 20x and 10x objectives.

Microscope characterization of silicon chips was conducted using a Zeiss AX10 microscope after 24 h of growth. A minimum of 3 images were taken at random locations over the top face of the substrate using bright field (BF) and dark field (DF) filters using a 10x objective.

3.2.2.4 Quantification of Growth Inhibition

The capability of the various peptide-loaded films to inhibit fungal growth was quantitatively assessed using 2,3-bis-(2-methoxy-4-nitro-5-sulfophenyl)-2H-tetrazolium-5-carboxanilide (XTT), which is reduced to a water-soluble dye by metabolically active cells. Chips were first gently transferred to a new chamber slide cassette. An XTT solution (0.5 g/L XTT in PBS, 1 μM menadione) was added to all occupied wells (675 μl/well), and the cassettes were sealed with parafilm and incubated at 37°C for 2 h. The liquid was collected and centrifuged at 2,000 rpm for 5 min and was aliquoted into 5 individual wells of a 96-well plate (100 μl/well). Absorbance at 490, the absorbance maximum for the water-soluble dye resulting from XTT reduction, and 600 nm was measured using a 96-well plate reader (BioTek) to quantify the reduced XTT and any cell contamination respectively. Growth inhibition was calculated using from the absorbance of the XTT product in the sterility control (A_{490}^{XTT}), the PEM embedded with peptide ($A_{490}^{peptide}$), the PEM without peptide ($A_{490}^{no\ peptide}$), and the background absorbance signal (A_{490}) with the following equation:

$$\%\ \text{Reduction in Metabolic Activity} = 100 \times \left[\frac{\left(A_{490} - A_{490}^{peptide}\right)}{\left(A_{490}^{no\ peptide} - A_{490}^{XTT}\right)}\right]$$

A one-way ANOVA or two-way ANOVA analysis followed by Tukey's multiple comparisons test (GraphPad Prism 8.01) was performed to statistically assess the impact of the drug-loaded PEMs on the reduction in metabolic activity of *C. albicans.*

3.3 Results

3.3.1 Scope of Research

Polyelectrolyte multilayer films (PEMs) were embedded with the peptides histatin 5 and K11RK17R (Table 3.1) were fabricated to assess their capability at preventing fungal adhesion and biofilm growth. The PEMs were fabricated via layer-by-layer deposition using 0, 1, and 3 mg/mL dipping solutions for each peptide and were tested in parallel with the same cell culture of *C. albicans*. These experiments were performed to explore potential routes of therapeutic administration for treating topical candidiasis.

3.3.2 Characterizing Film Thickness in Silicon Substrates

Thickness characterization was performed on all PEMs after fabrication to determine the approximate amount of peptide loaded onto each chip and the contribution of peptide to the thickness of the film. From these measurements, histatin 5 was shown to increase the thickness of the PEMs, adding approximately 45.85 ± 23.77 nm to the overall thickness of each chip. A lack of statistical significance between the thickness of the PEMs constructed using 1 mg/mL and 3 mg/mL dipping solutions of histatin 5 was also observed (Figure 3.3), indicating the thickness is not dependent on dose for these concentrations.

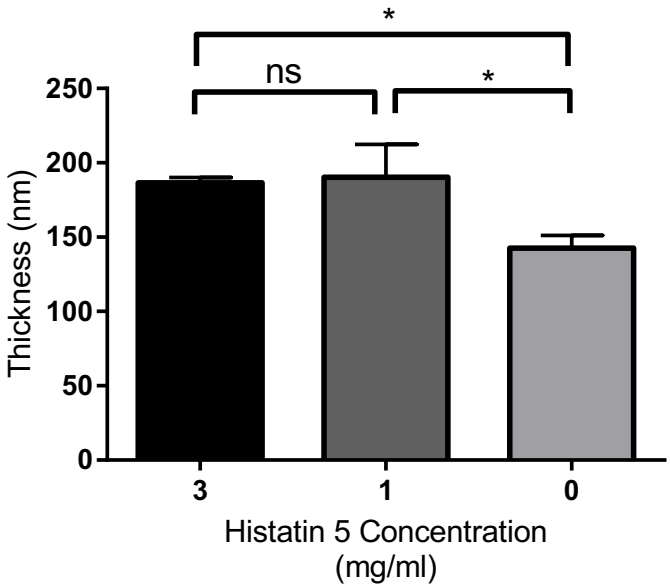

Figure 3.3: Thickness of Silicon Substrates with Films Post-Fabrication. All measurements displayed represents the average thickness with error bars corresponding to the standard deviation (n=3 chips). One-way ANOVA shows no statistically significant difference between 3 mg/mL and 1 mg/mL loading (ns) while a significant difference exists between films without histatin 5 (0 mg/mL) and those with histatin 5. The number of asterisks indicates the level of significance: * for $P<0.1$.

3.3.3 Biofilm Inhibition on Silicon Substrates

The ability of histatin 5-loaded PEMs to prevent *C. albicans* adhesion and proliferation was tested to determine if the fabricated PEMs on silicon substrates were efficacious. To assess this, chips with films fabricated using 0, 1, and 3 mg/mL of histatin 5 were incubated with *C. albicans* for 24 h. Following incubation, both microscopy analysis and quantification of growth inhibition was conducted.

3.3.3.1 Microscopy Analysis of Silicon Substrates

Microscopy was performed to analyze the relative amounts of fungal adhesion and growth on the exposed surface of the substrate (Figure 3.4).

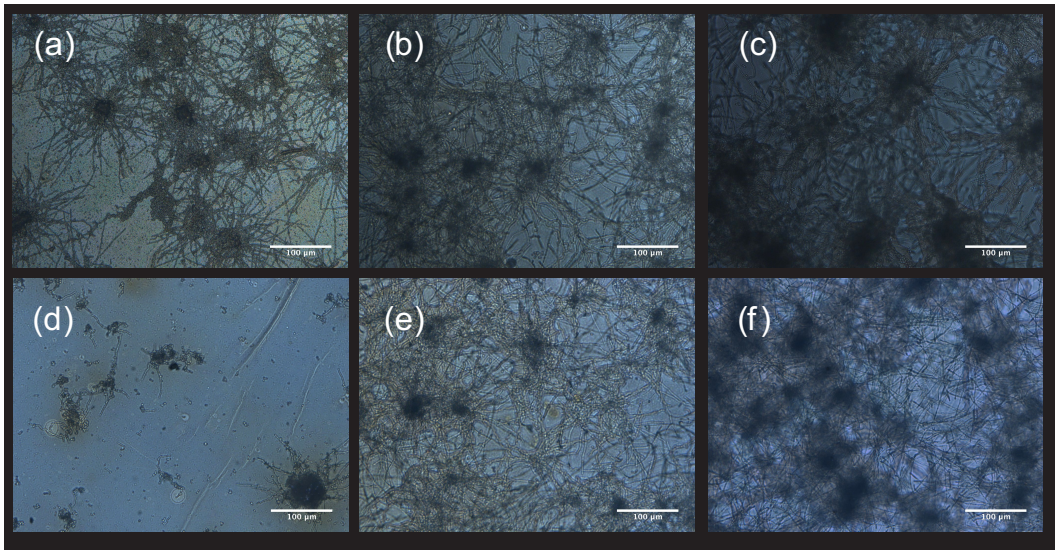

Figure 3.4: Microscope Images of Silicon Substrate PEMs. Images (a) – (c) correspond to silicon substrates dosed with 0, 1, and 3 mg/ml histatin 5 for the first trial. Images (d) – (f) correspond to silicon substrates dosed with 0, 1, and 3 mg/mL histatin 5 for the second trial. All presented images were taken with bright field objective and have scale bars equivalent to 100 μm.

No significant difference is visible in the adhesion or viability profiles as a function of histatin 5 concentration in the first trial, though there is a distinguishable increase in the presence of *C. albicans* yeast cells and hyphae in the peptide-loaded chips compared to the control in the second trial. The growth appears to be inversely proportional to peptide concentration, which was unexpected due to the well-established fungicidal activity of histatin 5.

3.3.3.2 Quantification of Growth Inhibition in Silicon Substrates

To validate the conclusions reached by microscopy analysis, quantitative viability analysis was performed with XTT to determine the relative metabolic activity of *C. albicans* on the surface of each chip (Figure 3.5). The metabolic activity of *C. albicans* in the supernatant was also measured as a precaution to help explain the findings observed with adherent cells and identify potential sources of error in the

experiment (Figure 3.6). From this analysis, the inverse concentration dependence was confirmed in both trials with significant differences in the relative metabolic activity of adherent *C. albicans* on the surface of either chip.

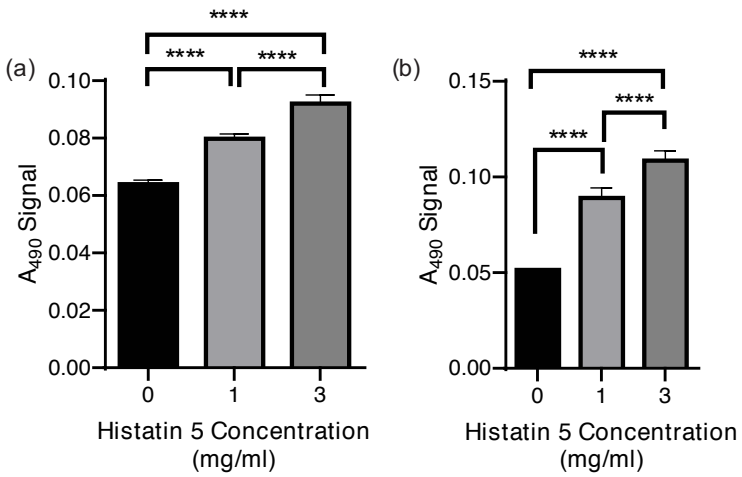

Figure 3.5: XTT Data for Growth on Silicon Substrates. (a) A_{490} absorbance measurements gathered from the first trial of PEM chips after 24 h of incubation and (b) A_{490} absorbance measurements gathered from the second trial of PEM chips after 24 h of incubation. All measurements displayed represent the average XTT signal for a single chip with error bars corresponding to the standard deviation (n=5). One-way ANOVA was performed to determine that the A_{490} signal increased with histatin 5 concentration. The number of asterisks indicates the level of significance: **** for $P<0.0001$.

Additionally, no significant differences in the metabolic activity of the supernatant was observed in the first trial (Figure 3.6a). This indicates that equivalent cellular viability is present in the supernatant of each PEM and that any peptide that diffused into the supernatant during incubation did not have a significant antifungal effect. Combine with the silicon substrate surface analysis, this indicates that integration of histatin 5 increased the biofilm growth on the surface of the chip and did not have a significant effect on preventing cellular adhesion.

This correlation was also present in the comparison between chips constructed with either 1 mg/mL or 3 mg/mL of histatin 5 in the second trial (Figure

3.5b). However, the control chip had significantly less metabolic activity in its supernatant, which could be indicative of a lower level of initial cell seeding on the surface or due to less release of cells into the supernatant from the surface or biofilm.

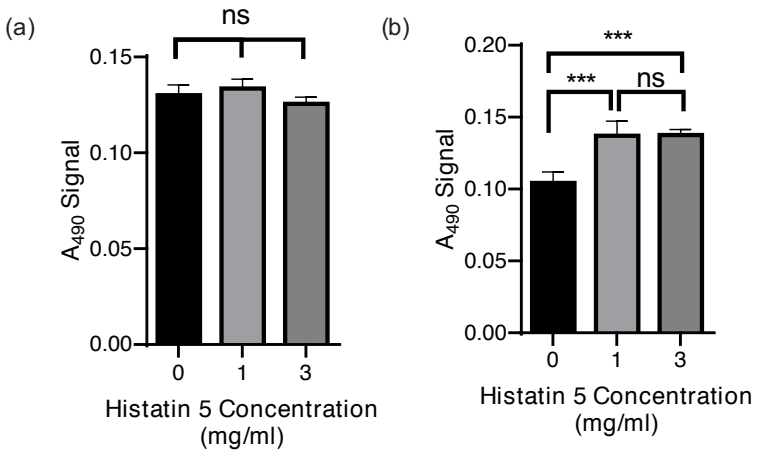

Figure 3.6: XTT Data for Silicon Chip Supernatants. (a) A_{490} absorbance measurements gathered from the supernatants of PEM chips in the first trial after 24 h of incubation and (b) A_{490} absorbance measurements gathered from the supernatants of PEM chips in the second trial after 24 h of incubation. All measurements displayed represent the average XTT signal for a single chip's supernatant with error bars corresponding to the standard deviation (n=5). One-way ANOVA was performed to determine that there was no statistically significant difference between the supernatant of all chips in the first trial (ns) and a statistically lower A_{490} signal in the control chip compared to the histatin 5 loaded chips in the second trial. The number of asterisks indicates the level of significance: *** for $P<0.001$.

To quantify and compare the capability of either peptide to inhibit the growth of *C. albicans* biofilms, the reduction in the metabolic activity can be used as a metric of comparison. Direct comparison of the capacity of each PEM to reduce the metabolic activity of the adherent *C. albicans* population was investigated within each independent trial (Figure 3.7). In both cases, the presence of peptide resulted in an increase in the metabolic activity of the adherent *C. albicans* with higher increases in metabolic activity being observed at higher concentrations of histatin 5.

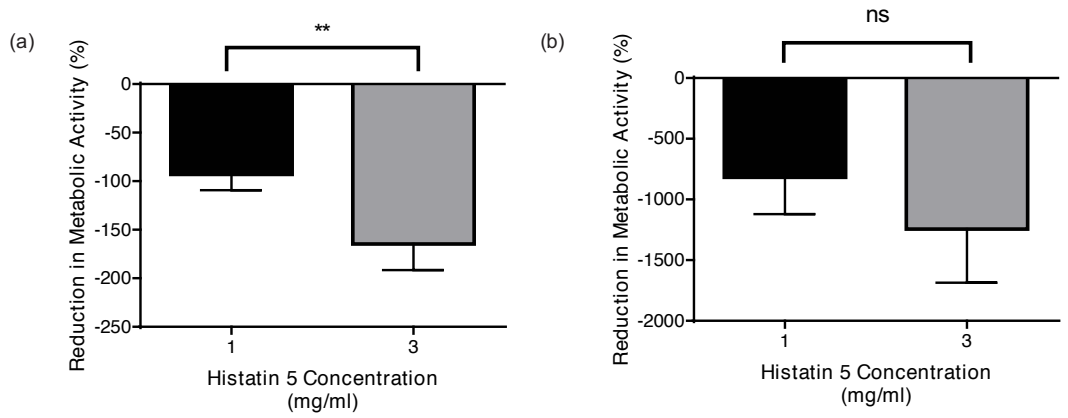

Figure 3.7: Reduction in Metabolic Activity for Silicon PEMs. (a) Reduction in metabolic activity calculated from the PEM chips in the first trial after 24 h of incubation and (b) reduction in metabolic activity calculated from the PEM chips in the second trial after 24 h of incubation. All measurements displayed represents the average reduction in metabolic activity based on that of a single chip with error bars corresponding to the standard deviation (n=5). A negative reduction in metabolic activity corresponds to an increase in biofilm growth. One-way ANOVA was performed to identify a significantly lower reduction in metabolic activity in the 3 mg/mL chip of the first trial compared to the 1 mg/mL chip and no significant difference in metabolic activity reduction in the second trial between the two chips (ns). The number of asterisks indicates the level of significance: ** for $P<0.01$.

3.3.4 Biofilm Inhibition on Quartz Substrates

Although experiments on silicon substrates provided initial evidence that incorporating histatin 5 has an effect on *C. albicans* growth, subsequent experiments were performed on quartz substrates for ease in microscopy analysis and to allow the acquisition of higher magnification images. PEMs were constructed in an identical manner to that performed with silicon substrates for this set of experiments. The peptide K11RK17R, which has a higher antifungal activity against *C. albicans* compared to histatin 5 [53], was also investigated in parallel to histatin 5 in these experiments to compare its biofilm inhibition performance. An initial 2 h seeding phase at 37°C was implemented to allow for sufficient surface adhesion and to more directly examine the effect of PEMs on inhibiting the biofilm growth and reducing

the metabolic activity of adherent cells. Following the seeding phase, chips were incubated at 37°C and removed at 6, 12, and 24 h to characterize the extent of biofilm proliferation and metabolic activity reduction due to the integration of either histatin 5 or K11RK17R in the PEM.

3.3.4.1 Microscopy Analysis of Quartz Substrates

Microscopy analysis was conducted for quartz substrates to assess the agreement of observations associated with histatin 5-loaded PEMs on silicon substrates with those on quartz substrates and to assess the ability of K11RK17R to prevent fungal adhesion and proliferation (Figure 3.8). In all cases, the qualitive comparison of performance on quartz substrates was much easier to discern due to the implementation of the initial seeding period. However, at 24 h, the imaging of these films became more difficult to perform due to the growth cell clumps in the supernatant, which cast a dark shadow on the surface of the substrate.

With regards to the histatin 5-loaded PEMs, an identical trend was observed here as was observed with the silicon substrates. In all cases, large, numerous biofilm networks are visible after 24 h regardless of the presence of histatin 5 in 1mg/mL or 3 mg/mL concentrations. Additionally, a visible difference in biofilm growth after only 6 h of incubation is present, indicating that histatin 5 may actually help in fungal colonization of the surface. This supports the previous silicon substrate findings and suggests that the integration of histatin 5 into PEMs can actually have a detrimental influence on preventing the colonization of *C. albicans.*

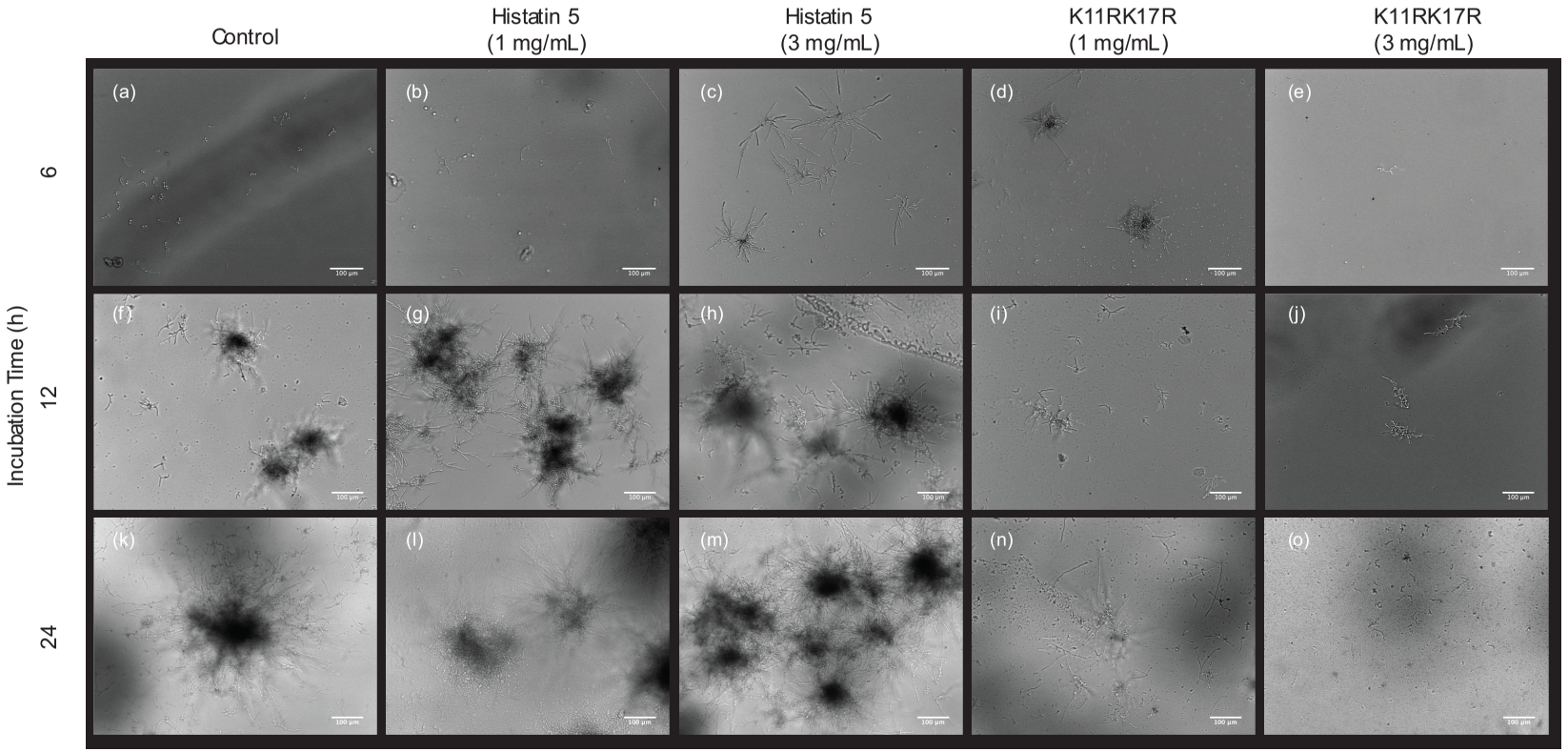

Figure 3.8: Microscope Images of Biofilm Formation on Quartz PEMs. (a) – (e) correspond to 0 mg/mL, histatin 5 at 1mg/mL, histatin 5 at 3 mg/ml, K11RK17R at 1mg/mL, and K11RK17R at 3 mg/mL at 6 hours, respectively. (f) – (j) correspond to 0 mg/mL, histatin 5 at 1mg/mL, histatin 5 at 3 mg/ml, K11RK17R at 1mg/mL, and K11RK17R at 3 mg/mL at 12 hours, respectively. (k) – (o) correspond to 0 mg/mL, histatin 5 at 1mg/mL, histatin 5 at 3 mg/ml, K11RK17R at 1mg/mL, and K11RK17R at 3 mg/mL at 24 hours, respectively. All images displayed were taken with the BF lens and are representative of the other photos taken of each chip at the same time point. All scale bars are equivalent to 100 μ m.

Meanwhile, K11RK17R exhibits efficient reduction of fungal growth on the surface, with only a small fraction of the present cells existing in the hyphal state after 24 h of incubation. This behavior is significant because the transition of *C. albicans* from yeast to hyphal states is a major virulence factor, which assists in the invasion of endothelial cells and in infection [78]. While some hyphal networks are visible on the PEMs fabricated with 1 mg/mL K11RK17R, these are still very small in comparison to the size of the networks observed on the control chips.

3.3.4.2 Quantification of Growth Inhibition in Quartz Substrates

The ability of K11RK17R and histatin 5 to inhibit *C. albicans* growth was quantified through XTT analysis and comparison in reduction of metabolic activity in an identical fashion to that performed with silicon substrates. In the case of histatin 5, PEMs that incorporate the peptide at 1 mg/mL are shown to reduce the metabolic activity of the cells in solution after 6 and 24 h of incubation (Figure 3.9a). Meanwhile, incorporating histatin 5 at 3mg/mL increases the metabolic activity of the cells after 6 and 24 h. The opposite is observed for PEMs constructed with K11RK17R with no significant difference in the reduction of metabolic activity between 6 and 24 h (Figure 3.9b). This indicates that there is a dose response present in for the treatment of *C. albicans* biofilms for histatin 5 with high concentrations significantly encouraging biofilm growth, which was also observed on silicon substrates. For K11RK17R, an opposite dose response is observed with high concentrations of K11RK17R reducing biofilm growth. Because there is no significant difference in metabolic reduction of K11RK17R PEMs constructed by 1

mg/mL and 3 mg/mL peptide, this indicates that these PEMs could continue to display similar performance in preventing biofilm formation after 24 h.

At 12 h the growth of biofilms on the surface of both K11RK17R and histatin 5 PEMs is significantly increased. This observation was made for a single biological replicate. Therefore, this does not confidently reflect the actual biofilm growth behavior of PEMs that were incubated for longer durations. While these observations do agree with the microscopy analysis for histatin 5 more so than that for K11RK17R, the large increase in metabolic activity is likely due to the large variance in A_{490} signal present at this time point, which translates to a large magnitude in cell growth (Supp. Figure B.1). Alternatively, the significantly high viability in the supernatant and on the chip at 12 h could indicate that the stability of the PEM is compromised between 12 and 24 h at 30°C. This would result in the release of peptide and adherent *C. albicans* into the supernatant, decreasing the metabolic activity observed on the surface of the PEMs and reducing supernatant viability through the antifungal action of the released peptide.

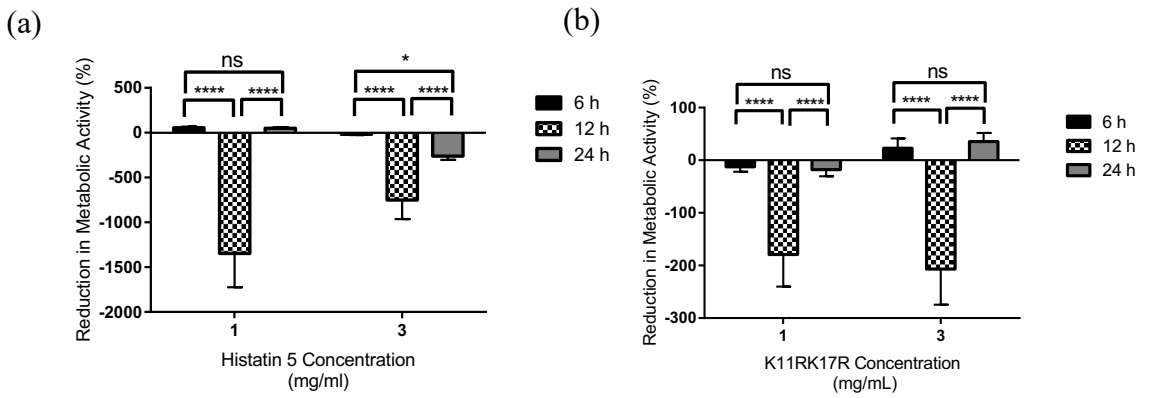

Figure 3.9: Reduction in Metabolic Activity in Histatin 5 and K11RK17R-Loaded Quart Chips. Reduction in metabolic activity calculated from histatin 5 (a) and K11RK17R-loaded (b) PEM chips fabricated on quartz substrate at 6, 12, and 24 h. All measurements displayed represents the average reduction in metabolic activity based on that of a single, individual chip for 6 and 12 h (n=1) and two chips for 24 h (n=2) with error bars corresponding to the standard deviation. A negative reduction in metabolic reduction corresponds to an increase in biofilm growth. The number of asterisks indicates the level of significance: * for P<0.01 and **** for P<0.0001.

Comparing the endpoint capability of histatin 5 and K11RK17R PEMs to prevent colonization and biofilm growth after 24 h of incubation, a stark difference in metabolic activity is observed (Figure 3.10). For example, high concentrations of histatin 5 can significantly help encourage biofilm growth. These observations are supported by microscopy analysis for the comparison of the control (Figure 3.8k) and 3 mg/mL film (Figure 3.8.m), which show more extensive biofilm growth on the 3 mg/mL substrate compared to the control. The reduction in metabolic activity demonstrated in the XTT analysis by the 1 mg/mL histatin 5 substrate (Figure 3.8l) is difficult to validate with microscopy as both chips show approximately equivalent biofilm growth. Meanwhile, the high concentrations of K11RK17R embedded in PEMs results in a significant increase in metabolic reduction. This is supported by microscopy analysis as significantly more biofilm growth is visible on the control (Figure 3.8k) compared to the 3mg/mL K11RK17R chip (Figure 3.8o) at 24 h. In the

case of the 1 mg/mL K11RK17R substrate (Figure 3.8n), findings from the XTT analysis contradict with microscopy findings. This is reconciled by the large variance in the calculated reduction of metabolic activity for this sample, which suggests that the inhibition of biofilm formation is minimal in comparison to the control. In general, this indicates that the K11R and K17R mutations initially found to improve the proteolytic stability of histatin 5 may also provide additional fitness advantages for the incorporation into polyelectrolyte multilayer films with dipping solutions at high concentrations of peptide.

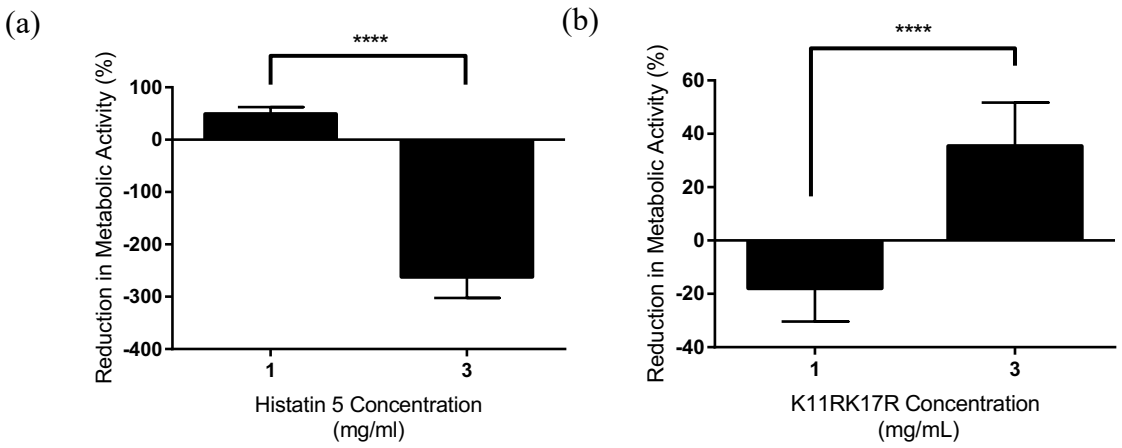

Figure 3.10: Endpoint Reduction in Metabolic Activity. (a) Reduction in metabolic activity calculated from the quartz, histatin 5-loaded PEM chips after 24 h of incubation and (b) reduction in metabolic activity calculated from the quartz, K11RK17R-loaded PEM chips after 24 h of incubation. All measurements displayed represents the average reduction in metabolic activity based on that of two individual chips with error bars corresponding to the standard deviation (n=2). A negative reduction in metabolic reduction corresponds to an increase in biofilm growth. One-way ANOVA was performed to determine that higher concentrations of histatin 5 correlate to a lower reduction in metabolic activity while the opposite is true for K11RK17R. The number of asterisks indicates the level of significance: **** for $P<0.0001$.

3.4 Discussion

Integration of histatin 5 in PEMs deposited on both silicon and quartz substrates resulted in an increase in *C. albicans* biofilm formation and metabolic activity on the

surface, which increased with loading peptide concentration. This observation was supported by both microscopy and XTT analyses. These findings were unexpected as prior work demonstrated that histatin 5 has antifungal properties and can be used to inhibit C. albicans biofilm formation [33, 40, 42, 53]. Furthermore, histatin 5 has been integrated into hydrogels for topical treatment of *C. albicans* [83]. This indicates that integrating histatin 5 into PEMs can significantly influence the activity of the peptide and that dehydrated storage of histatin 5 could have a detrimental influence on its antifungal activity.

Alternatively, the unexpected observations made with respect to histatin 5 in these experiments could be due to errors in PEM fabrication. For example, the thickness of the PEMs deposited on silicon in these experiments were 10-fold thinner than those constructed with 60 (PGA-β-peptide-PLL)$_n$ trilayers in another study [80]. Highly variable loading was also observed in comparison of peptide dipping solutions before and after PEM fabrication (Supp. Figure B.2) as well as the A_{280} absorbance from chip-to-chip after PEM fabrication (Supp Figure B.3). Therefore, it is likely that insufficient amounts of histatin 5 was loaded onto each chip during fabrication, resulting in lower than expected antifungal activity. To verify this, stability and release studies should be conducted. Future works should optimize the PEM fabrication process to ensure peptide loading levels and film characteristics are consistent with expected findings. Alternatively, different polymers could be considered to encourage peptide integration. Since PGA/PLL PEMs are an example of exponentially growing films, weak electrostatic interactions exist between the polyanion and polycation and allow for easy absorption and desorption of polymer

and peptide during wash steps [75]. On the other hand, linearly growing PEMs, such as those produced by poly(styrenesulfonate)/poly(allylamine) $(PSS/PAH)_n$, are characterized by stronger electrostatic interactions and are highly stratified and could be used to potentially increase peptide loading [75]. Alternatively, PGA could be removed from the PEM fabrication process, relying solely on the positive charge of the antifungal peptide to generate the polycation portion of the bilayer.

Compared to histatin 5, K11RK17R demonstrated significantly higher biofilm inhibition at high concentrations, which was observed in both microscopy and XTT analysis. Meanwhile, PEMs prepared from 1 mg/mL of K11RK17R exhibited only minor biofilm inhibition at low concentrations with microscopy analysis. These observations were not supported by XTT analysis and are most likely due to small differences in A_{490} signal. Therefore, future work should aim to improve the XTT assay by increasing the seeding of *C. albicans* and subsequentially the contrast in metabolic activity between concentrations of peptide. Alternatively, increasing the number of replicates could lead to improved differentiation and result in more significantly different biofilm inhibition.

Chapter 4: Conclusions and Future Work

4.1 Conclusion

In Chapter 2, the antifungal peptide histatin 5 was successfully integrated into a yeast surface display system and was shown to be degradable by Saps 2 and 9 while expressed as a part of a fusion protein. It was also shown that the degradation of the peptide could be influenced by changing the degradation conditions including the proportion of protease to cells as well as the buffer, pH, temperature, and time of incubation. Optimization resulted in the identification of new conditions that improved the resolution between proteolytically stable (K11RK17R) and proteolytically susceptible (K13L) variants of histatin 5. Now that we have a better understanding of the system, further improvement can be performed to improve the stringency of this system. Therefore, it is promising that this system could be used to screen for novel variants with enhanced proteolytic stability produced using directed evolution.

In Chapter 3, a study was performed where histatin 5 and the double mutant K11RK17R were integrated into polyelectrolyte-multilayer films (PEMs) on both silicon and quartz substrates and used to inhibit *C. albicans* biofilm formation. From this study, it was observed that K11RK17R could significantly reduce the metabolic activity of *C. albicans* and reduce biofilm formation after 24 h, while the opposite was observed for histatin 5, which increased *C. albicans* growth and biofilm formation. While fabrication of the PEMs requires optimization in later studies to

improve the loading of peptide on either substrate, this study shows that the peptide can be successfully incorporated and potentially used to prevent infection.

4.2 Future Work

4.2.1 Improving the Proteolytic Stability of Histatin 5

The yeast surface display system developed and optimized in this study can be used to identify novel variants of histatin 5 with improved proteolytic stability. This can be accomplished by using degenerate primers to introduce random mutations into histatin 5 at amino acid positions of interest and screening for resulting peptide with improved proteolytic stability using Sap2 and Sap9. Given that a significant improvement in the proteolytic stability of histatin 5 was imparted by K11R and K17R mutations, further investigation should primarily be investigated at these positions. The primers required to sample all amino acids at the K11 position can be used with the QuickChange II site-directed mutagenesis kit (Agilent) are displayed in Table 4.1 below. Similarly, the primers required to sample all amino acids at the K17 position can be used with the same kit and are displayed in Table 4.2 below.

Table 4.1: Degenerate Primers for K11 Mutagenesis

Primer	Sequence (5' to 3')
a36n_a37n_g38n_top	atgcaaaacgccatcacgggtat**nnn**cgcaagttccacgaaaagc
a36n_a37n_g38n_bot	gcttttcgtggaacttgcg**nnn**atacccgtgatggcgttttgcat

Table 4.2: Degenerate Primers for K17 Mutagenesis

Primer	Sequence (5' to 3')
a54n_a55n_g56n_top	ataagcgcaagttccacgaa**nnn**caccacagtcatcgcggg
a54n_a55n_g56n_bot	cccgcgatgactgtggtgnnnttcgtggaacttgcgcttat

The neighboring amino acids to K11 and K17 should also be investigated as the side chains of these residues can influence the accessibility of K11 and K17 by Saps,

possibly preventing recognition and subsequent degradation. The mutants identified with enhanced proteolytic stability should then be used to treat *C. albicans* in an identical fashion to previous studies to ensure that the mutations do not compromise antifungal activity [53].

4.2.2 Alternative Methods to Improve Proteolytic Stability

While it was shown in this study that the peptide can be expressed in a yeast surface display system and interrogated with Saps without significantly compromising the viability of the yeast cell, dosing the cells with Saps does not ensure that each fusion is interrogated. To mitigate this issue, the yeast endoplasmic-reticulum sequestration screening (YESS) system can be used instead of traditional yeast surface display. YESS addresses this issue of adequate Sap interrogation by simultaneously expressing a similar yeast surface display fusion along with a protease using the divergent GAL1,10 promoter, which is shown in Figure 4.1 [84]. The additional expression of the protease ensures that the fusion protein is interrogated by the protease in the endoplasmic reticulum before being translocated to the cell wall, negating the need to supplement the cells with purified protease and significantly reducing the required time and resources by performing digestion during expression. Though originally designed to screen for proteases with enhanced activity, this system could also be used to improve the proteolytic stability of histatin 5.

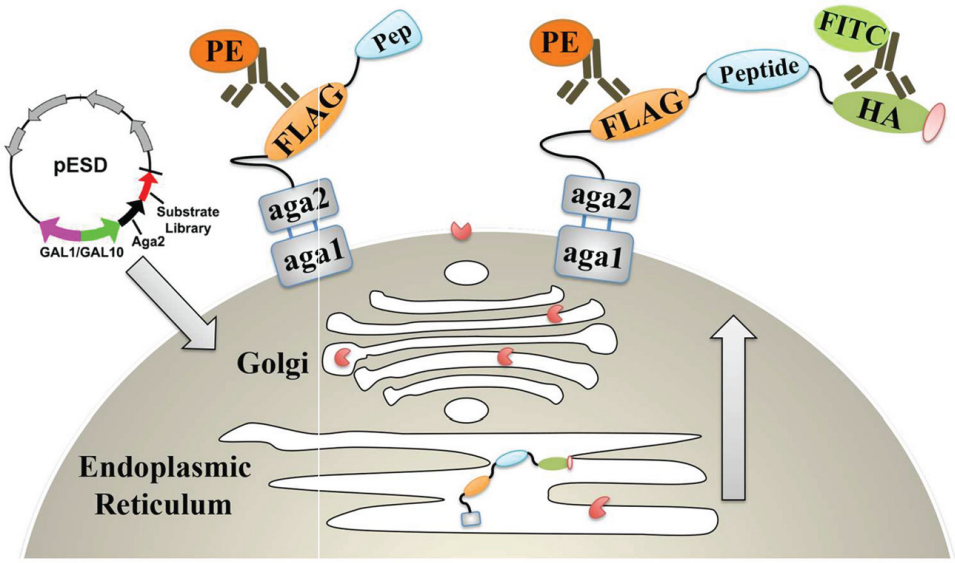

Figure 4.1: Illustration of YESS System. Figure is modified with permission from [84]. Copyright 2017 American Chemical Society. A divergent galactose-inducible promoter (pGAL1-pGAL10) controls the expression of the substrate and protease library. The peptide library consists of a terminal HA tag followed by the peptide of interest, a FLAG epitope tag, and Aga2 protein to anchor the fusion to the cell wall through association with Aga1. The protease is expressed to the endoplasmic reticulum to interrogate the fusion during expression. Both FLAG and HA tags are detectable with antibodies, allowing for degradation analysis with flow cytometry and FACS.

4.2.3 *In Vivo* Testing of Fabricated PEMs

Given the observed improvement in biofilm inhibition observed by the PEM fabricated with a 3 mg/mL K11RK17R dipping solution, *in vivo* testing should be performed to progress its therapeutic development. This could be accomplished by depositing the K11RK17R-embedded PEMs on a disk and observing its ability to inhibit oral fungal infection in a mouse model, which was previously performed by another group using an identical PGA/PLL PEM system embedded with poly(methylmethacrylate) and chromofungin [85].

Prior to in vivo testing, more characterization is also required for the PEMs developed in this study. This includes characterizing the drug-release profiles for

these chips and the stability of the PEMs. Both of these properties are commonly investigated in other studies [80, 81, 86]. By studying the drug-release profile of these PEMs, the true endpoint at which biofilm inhibition is no longer inhibited can be determined. Additionally, the stability of the chip in serum, saliva, and water will assist in determining the stability of the chip in these environments, which may influence their rate of drug release. By studying both of these parameters, further confidence in the performance of our PEMs can be gained.

Additionally, optimization the construction process is required for the PEMs investigated in this study to ensure even and sufficient drug loading from chip-to-chip. Optimization of this process may also improve the efficacy of the histatin 5 loaded PEMs, as their failure to inhibit biofilm formation was likely due to insufficient loading. Alternatively, it may be worthwhile to reduce the trilayers (PGA-peptide-PLL)$_n$ to bilayers (Peptide-PLL)$_n$, as removing the polycation species could ensure a higher loading of the peptide to the chip due to electrostatic association. In either case, the PEMs investigated in this study show promise for in vivo therapeutic application and should be further investigated as a novel treatment for the prevention of *C. albicans* infections.

Appendix A – Supplemental Figures (Chapter 2)

Table A.1: Raw Data for Influence of pH on Sap2 and Sap9

Peptide	Sap	pH	% Myc + Events	C-Myc Signal*	% Myc – Events	C-Myc Signal*
K11RK17R	2	7.0	67.26	19192 ± 26202	32.74	82.5 ± 87.2
		4.0	61.3	15343 ± 23871	38.7	85.9 ± 86
	9	7.0	65.45	21949 ± 3115	34.55	85.4 ± 87.2
		5.0	63.26	18011 ± 25488	36.74	74.5 ± 86.1
K13L	2	7.0	71.4	2394 ± 3728	28.53	76.4 ± 7.2
		4.0	52.53	3817 ± 6108	47.47	91 ± 86.3
	9	7.0	62.99	3762 ± 5362	37.01	96.7 ± 89.9
		5.0	61.85	5380 ± 6336	38.15	91.8 ± 87.6

* All values represent the average intensity determined from a single biological replicate ± the standard deviation in the population (n=1).

Table A.2: Raw Data for Scale Down Analysis of pCTcon2-Hst5

Cell Count (x 10^6)	Sap2 Concentration (μg/mL)	Q1 (HA+/Myc-)*		
		%Events	HA Signal	C-Myc Signal
2	200	8.27 ± 1.66	3447 ± 5258	133 ± 190
	1000	9.75 ± 2.68	4412 ± 7351	136 ± 175
4	200	6.64 ± 1.61	3528 ± 6242	136 ± 197
	1000	8.18 ± 0.82	3788 ± 5750	125 ± 237
		Q2 (HA+/Myc+)*		
		%Events	HA Signal	C-Myc Signal
2	200	60.67 ± 15.93	51138 ± 89422	6665 ± 18714
	1000	62.10 ± 10.74	46786 ± 77260	4462 ± 14168
4	200	65.27 ± 6.70	64494 ± 99633	8149 ± 21876
	1000	65.47 ± 6.77	67879 ± 95496	5692 ± 15914

*Values represent the average of three biological replicates ± the standard deviation in the population (n=3).

Table A.3: Raw Q2 Data of Histatin 5 Degraded at 2, 4, 6 h and 30°C and 37°C

Incubation Time (h)	Incubation Temperature (°C)	% Events*	HA Signal*	C-Myc Signal*
0	30	66.50 ± 21.71	48121 ± 78549	6381 ± 19763
	37	59.35 ± 2.57	48859 ± 84649	5993 ± 18038
2	30	64.70 ± 7.41	61579 ± 73232	4323 ± 13611
	37	66.67 ± 7.52	54558 ± 65604	4454 ± 13610
4	30	63.13 ± 12.72	55254 ± 63359	3104 ± 12510
	37	67.00 ± 2.51	56514 ± 66316	3050 ± 9245
6	30	56.70 ± 8.35	42417 ± 58393	2136 ± 12012
	37	63.1 ± 2.27	48120 ± 59457	2877 ± 9159

*Values represent the average of three biological replicates ± the standard deviation in the population (n=3).

Appendix B – Supplemental Figures (Chapter 3)

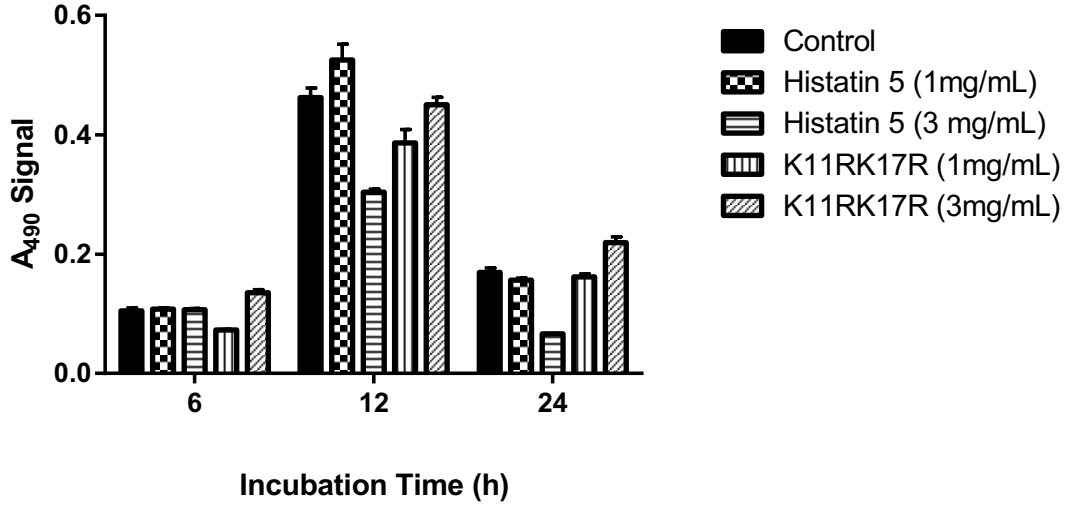

Figure B.1: Relative A_{490} for Quartz PEM Supernatants. The average A_{490} signal, corresponding to that of XTT, is shown for both histatin 5 and K11RK17R-loaded quartz PEM chips based on a single chip at 6 h and 12 h (n=1) and two chips at 24 h (n=2). Error bars represent the standard deviation in the populations.

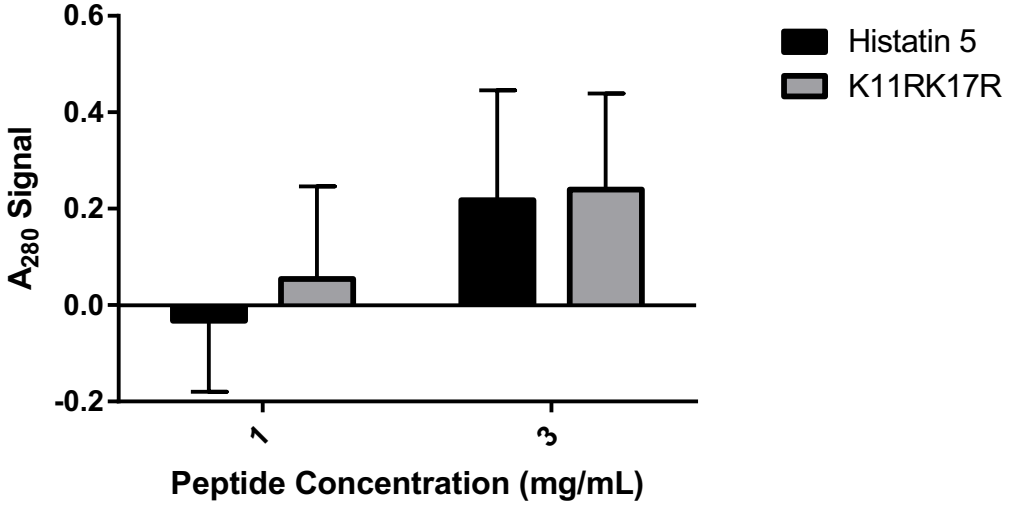

Figure B.2: Absorbance Differences in Peptide Dipping Solutions Pre- and Post-Fabrication. The plotted signal represents the difference in the absorbance at 280 nm (A_{280}) between the peptide dipping solutions before and after centrifuging after fabrication. The average difference in A_{280}, is shown calculated from n=3 chips for histatin 5 and n=4 chips for K11RK17R with error bars representing the standard deviation.

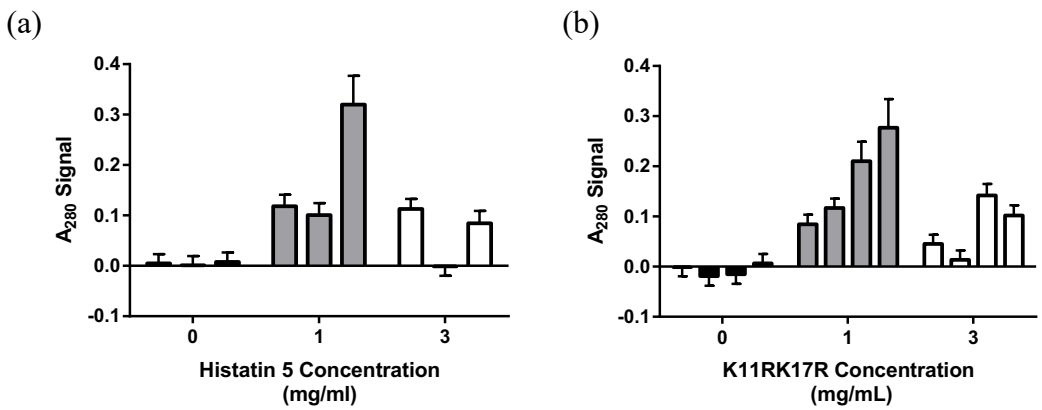

Figure B.3: Absorbance of PEM Films Post-Fabrication. The absorbance at 280 nm was measured for each PEM fabricated on quartz substrate with (a) histatin 5 and (b) K11RK17R to get an estimate of the peptide loading in a given chip. Triplicate measurements were performed for each chip (n=3). The data graphed represent averages for each PEM chip with error bars representing the standard deviation of the populations.

References

[1] Armstrong, A. W., Bukhalo, M., Blauvelt, A. A clinician's guide to the diagnosis and treatment of candidiasis in patients with psoriasis. *Am J Clin Dermatology*. **2016**, 17(4), pp. 329-36.

[2] Li, C., Lee, R., Wang, Y., Zheng, X., Wang, Y. *Candida albicans* hyphal morphogenesis occurs in Sec3p-independent and Sce3p-dependent phases separated by septin ring formation. *J Cell Science.* **2007**, 120(Pt 11), pp. 1898-907.

[3] Pappas, P. G., Lionakis, M. S. Arendrup, M. C., Ostrosky-Zeichner, L., Kullberg, B. J. Invasive candidiasis. *Nat Rev Dis Primers*. **2018**, 4:18026.

[4] McManus, B. A., Coleman, D. C. Molecular epidemiology, phylogeny and evolution of *Candida albicans*. *Infect Genet Evol.* **2014**, 21, pp. 166-78.

[5] Toeh, F., Pavelka, N. How chemotherapy increases the risk of systemic candidiasis in cancer patients: current paradigm and future directions. *Pathogens*. **2016**, 5(1), pp. 1-16.

[6] Shosham, S. Marr, K. A. Invasive fungal infections in solid organ transplant recipients. *Future Microbiology*. **2012**, 7(5), pp. 639-55.

[7] Marr, Kieren A. Future infections in hematopoietic stem cell transplant recipients. *Medical Mycology*. **2008**, 46(4), pp. 293-302.

[8] Rodrigues, C. F., Rodrigues, M. E., Henriques, M. *Candida* sp. Infections in patients with diabetes mellitus. *J Clin Med*. **2019**, 8(1), pp. 1-41.

[9] Armstrong-James, D., Meintjes, G., Brown, G. D. A neglected epidemic: fungal infections in HIV/AIDS. *Trends Microbiol*. **2014**, 22(3), pp. 120-27.

[10] Aguin, T. J., Sobel, J. D. Vulvovaginal candidiasis in pregnancy. *Curr Infect Dis Rep*. **2015**, 17(6), pp. 462.

[11] Morgan, J., Meltzer, M. I., Plikaytis, B. D., Sofair, A. N., Huie-White, S., Wilcox, S., Harrison, L. H., Seaberg, E. C., Hajjeh, R. A., Teutsch, S. M. Excess mortality, hospital stay, and cost due to candidemia: a case-control study using data from population-based candidemia surveillance. *Infect Control Hosp Edipemiol*. **2005**, 26(6), pp. 540-47.

[12] Kullberg, B. J., Arendrup, M. C. Invasive Candidiasis. *N Engl J Med*. **2015**, 373(15), pp. 1445-56.

[13] Walker, L. A., Gow, N. A., Munro, C. A. Fungal echinocandin resistance. *Fungal Genet Biol*. **2010**, 47(2), pp. 117-26.

[14] Perlin, D. Echinocandin Resistance in *Candida*. *Clin Infect Dis*. **2015**, 61(Supp 6), pp. 12-17.

[15] Garcia-Cuesta, C., Sarrion-Pérez, M. G., Bagán, J. V. Current treatment of oral candidiasis: a literature review. *J Clin Exp Dent*. **2014**, 6(5), pp. 576-82.

[16] Whaley, S. G., Berkow, E. L., Rybak, J. M., Nishimoto, A. T., Barker, K. S., Rogers, P. D. Azole antifungal resistance in C*andida albicans* and emerging non-albicans candida species. *Front Microbiol*. **2017**, 7:2173.

[17] Sanguinetti, M. Posteraro, B. Lass-Flörl, C. Antifungal drug resistance among candida species: mechanisms and clinical impact. *Mycoses*. **2015**, 58, pp. 2-13.

[18] Center for Disease Control and Prevention. Antibiotic Resistance Threats in the United States. **2013**. pp. 63-64.

[19] Vincent, B. M., Lancaster, A. K., Scherz-Shouval, R., Whitesell, L., Lindquist, S. Fitness trade-offs restrict the evolution of resistance to amphotericin B. *PLOS Biology*. **2013**, 11(10), e1001692.

[20] Martel, C. M., Parker, J. E., Bader, O., Weig, M., Gross, U., Warrilow, A. G., Kelly, D. E., Kelly, S. L. A clinical isolate of *Candida albicans* with mutations in ERG11 (encoding sterol 14α-demethylase) and ERG5 (encoding C22 Desaturase) is cross resistant to azoles and amphotericin B. *Antimicrob Agents Chemother*. **2010**, 54(9), pp. 3578-83.

[21] Sanati, H., Ramos, C. F., Bayer, A. S., Ghannoum, M. A. Combination therapy with amphotericin B and fluconazole against invasive candidiasis in neutropenic-mouse and infective-endocarditis rabbit models. *Antimicrob Agents Chemother*. **1997**, 41(6), pp. 1345-48.

[22] Cohen, B. E. Amphotericin B toxicity and lethality: a tale of two channels. *Int J Pharm*. **1998**, 162(1-2), pp. 95-106.

[23] Deray, G. Amphotericin B nephrotoxicity. *J Antimicrob Chemother*. **2002**, 49, pp. 37-41.

[24] Vila, T., Romo, J. A., Pierce, C. G., McHardy, S. F., Saville, S. P., Lopez-Ribot, J. L. Targeting candida albicans filamentation for antifungal drug development. *Virulence*. **2017**, 8(2), pp. 150-58.

[25] Forsberg, K., Woodworth, K., Walters, M., Berkow, E., Jackson, B., Chiller, J., Vallabhaneni, S. *Candida auris*: the recent emergence of a multidrug-resistant fungal pathogen. *Medical Mycology*. **2018**, 57(1), pp.1-12.

[26] Perlin, D. S., Rautemaa-Richardson, R. Alastruey-Izquierdo, A. The global problem of antifungal resistance: prevalence, mechanisms, and management. *Lancet Infect Dis*. **2017**, 17(12), pp. 383-392.

[27] Chowdhary, A., Sharma, C., Jacques, M. F. *Candida auris*: a rapidly emerging cause of hospital-acquired multidrug-resistant fungal infections globally. *PLOS Pathogens*. **2017**, 13(5), e1006290.

[28] Fosgerau, K., Hoffman, T. Peptide therapeutics: current status and future directions. *Drug Discov Today*. **2015**, 20(1), pp. 122-28.

[29] Reddy, K. V., Yedery, R. D., Aranha, C. Antimicrobial peptides: premises and promises. *Int J Antimicrob Agents*. **2004**, 24(6), pp. 536-47.

[30] Ng, S., Yap, Y., Cheong, J., Ng, F., Lau, Q., Barkham, T., Teo, J., Hill, J., Chia, C. Antifungal peptides: a potential new class of antifungals for treating vulvovaginal candidiasis caused by fluconazole-resistant *Candida albicans*. **2017**, 23(3), pp. 215-221.

[31] Mahlapuu, M., Kåkansson, J., Ringstad, L., Björn, C. Antimicrobial peptides: an emerging category of therapeutic agents. *Front Cell Infect Microbiol*. **2016**, 194(6), pp. 1-12.

[32] Lau, J., Dunn, M. Therapeutic peptides: Historical perspectives, current development trends, and future directions. *Bioorg Med Chem*. **2018**, 26(10), pp. 2700-07.

[33] Puri, S., Edgerton, M. How does it kill?: understanding the candidacidal mechanism of salivary histatin 5. *Eukaryotic Cell*. **2014**, 13(8), pp. 958-64.

[34] Oppenheim, F., Xu, T., McMillian, F., Levitz, S., Diamond, R., Offner, G., Troxler, R. Histatins, a novel family of histidine-rich proteins in human parotid secretion. Isolation, characterization, primary structure, and fungistatic effects on C*andida albicans*. *J Biol Chem*. **1988**, 263(16), pp. 7472-77.

[35] Swidergall, M., Ernst, J. Interplay between *Candida albicans* and the antimicrobial peptide armory. *Eukaryotic Cell*. **2014**, 13(8), pp. 950-957.

[36] Li, R., Kumar, R., Tati, S., Puri, S., Edgerton, M. *Candida albicans* Flu1-mediated efflux of salivary histatin 5 reduces its cytosolic concentration and fungicidal activity. *Antimicrob Agents Chemother*. **2013**, 57(4), pp. 1832-39.

[37] Du, H., Puri, S., McCall, A., Norris, H., Russo, T., Edgerton, M. Human salivary protein histatin 5 has potent bactericidal activity against ESKAPE pathogens. *Front Cell Infect Microbiol*. **2017**, 7(41), pp. 1-12.

[38] Mayer, F., Wilson, D., Jacobsen, I., Miramón, P., Grobe, K. Hube, B. The novel *Candida albicans* transporter Dur31 is a multi-stage pathogenicity factor. *PLOS Pathogens*. **2012**, 8(3), pp. 1-18.

[39] Kumar, R., Chadha, S., Saraswat, D., Bajwa, J., Li, R., Conti, H., Edgerton, M. Histatin 5 uptake by *Candida albicans* utilizes polyamine transporters Dur3 and Dur31 proteins. *J Biol Chem*. **2011**, 286(51), pp. 43748-58.

[40] Liao, H., Liu, S., Wang, H., Su, H., Liu, Z. Efficacy of histatin 5 in a murine model of vulvovaginal candidiasis caused by *Candida albicans*. *Pathogens and Disease.* **2017**, 75(6), pp. pp. 1-10.

[41] Xu, T., Levitz, S., Diamond, R., Oppenheim, F. Anticandidal activity of major human salivary histatins. *Infect Immun*. **1991**, 59(8), pp. 2549-54.

[42] Curvela, J. Moraes, D., Anjos, C., Portela, M., Soares, R. Histatin 5 and human lactoferrin inhibit biofilm formation of a fluconazole resistant *Candida albicans* clinical isolate. *Biological Sciences*. **2019**, 9(1), pp. 1-7.

[43] Moffa, E., Mussi, M., Xiao, Y., Garrido, S., Machado, M., Giampaolo, E., Siqueira, W. Histatin 5 inhibits adhesion of *C. albicans* to reconstructed human oral epithelium. *Front Microbiol*. **2015**, 6:885.

[44] Vylkova, S., Jang, W., Li, W., Nayyar, N., Edgerton, M. Histatin 5 initiates osmotic stress response in *Candida albicans* via activation of the Hog1 mitogen-activated protein kinase pathway. *Eukaryotic Cell*. **2007**, 6(10), pp. 1876-88.

[45] Silva, P., Goncalves, S., Santos, N. Defensins: antifungal lessons from eukaryotes. *Front Microbiol*. **2014**, 5(97), pp. 1-17.

[46] Pierce, C. G., Lopez-Ribot, J. L. Candidiasis drug discovery and development: new approaches targeting virulence for discovering and identifying new drugs. *Expert Opin Drug Discov*. **2013**, 8(9), pp. 1117-26.

[47] Da Silva Dantas, A., Lee, K., Raziunaite, I., Schaefer, K., Wagener, J., Yadav, B., Gow, N. Cell bioloby of *Candida albicans*-host interactions. *Curr Opin Microbiol.* **2016**, 34, pp. 111-18.

[48] Albrecht, A., Felk, A., Pichova, I., Naglik, J., Schaller, M., de Groot, P., Maccallum, D., Odds, F., Schafer, W., Klis, F., Monod, M., Hube, B. Glycosylphosphatidylinositol-anchored proteases of *Candida albicans* target proteins necessary for both cellular processes and host-pathogen interactions. *J Biol Chem*. **2006**, 281(2), pp. 688-94.

[49] Naglik, J., Challacombe, S., Hube, B. *Candida albicans* secreted aspartyl proteinases in virulence and pathogenesis. *Microbiol Mol Biol Rev*. **2003**, 67(3), pp. 400-28.

[50] Naglik, J., Moyes, D., Makawana, J., Kanzaria, P., Tsichlaki, E., Weindl, G., Tappuni, A., Rodgers, C., Woodman, A., Challacombe, S., Schaller, M., Hube B. Quantitative expression of the *Candida albicans* secreted aspartyl proteinase gene family in human oral and vaginal candidiasis. *Microbiology*. **2008**, 154(Pt 11), pp. 3266-80.

[51] Aoki, W., Kitachara, N., Miura, N., Morisaka, H., Yamamoto, Y., Kuroda, K., Ueda, M. Comprehensive characterization of secreted aspartic proteases encoded by a virulence gene family in *Candida albicans*. *J Biochem*. **2011**, 150(4), pp. 431-38.

[52] Koelsch, G., Tang, J., Low, J., Monod, M., Jackson, K., Foundling, S., Lin, X. Enzymic characteristics of secreted aspartic proteases of *Candida albicans*. *Biochim Biophys Acta.* **2000**, 1480(1-2), pp. 117-31.

[53] Ikonomova, S. P., Moghaddam-Taaheri, P. Jabra-Rizk, M. A., Wang, Y., Karlsson, A. J. Engineering improved variants of the antifungal peptide histatin 5 with reduced susceptibility to *Candida albicans* secreted aspartic proteases and enhanced antimicrobial potency. *FEBS J*. **2018**, 285(1), pp. 146-59.

[54] Meiller, T., Hube, B., Schild, L., Shirtliff, M., Scheper, M., Winkler, R., Ton, A., Jabra-Rizk, M.A. A novel immune evasion strategy of *Candida albicans*: proteolytic cleavage of a salivary antimicrobial peptide. *PLOS One*. **2009**, 4(4), pp. 1-9.

[55] Ikonomova, S.P., Moghaddam-Taaheri, P., Wang, Y., Doolin, M.T., Stroka, K.M., Hube, B., Karlsson, A.J. Effect of histatin-5 modifications on antifungal activity and kinetics of proteolysis. Submitted.

[56] Lehmann, M., Wyss, M. Engineering proteins for thermostability: the use of sequence alignments versus rational design and directed evolution. *Curr Opin Biotechnol.* **2001,** 12(4), pp.371-75.

[57] Yokobayashi, Y., Weiss, R., Arnold, F. Directed evolution of a genetic circuit. *PNAS*. **2002**, 99(26), pp. 16587-91.

[58] Baeriswyl, V., Heinis, C. Phage selection of cyclic peptide antagonists with increased stability toward intestinal proteases. *Protein Engr Des Sel*. **2012**, 26(1), pp. 81-89.

[59] McGlinchey, R., Lee, J. Cysteine cathepsins are essential in lysosomal degradation of α-synuclein. *PNAS*. **2015**, 112(30), pp. 9322-27.

[60] Boder, E. T., Wittrup, K. D. Yeast surface display for screening combinatorial polypeptide libraries. *Nat Biotechnol*. **1997**, 15(6), pp. 553-57.

[61] Vliet, L., Colin, P., Hollfelder, F. Bioinspired genotype-phenotype linkages: mimicking cellular compartmentalization for the engineering of functional proteins. *Interface Focus*. **2015**, 5(4), pp. 1-9.

[62] Sheehan, J., Marasco, W. Phage and yeast display. *Microbiol Spectr*. **2015**, 3(1), pp. 1-17.

[63] Lipovsek, Dasa, et al. "Library Construction for Protein Engineering." Protein Engineering and Design, edited by Marco Mena, CBC Press, **2010**, pp. 84–103.

[64] Cherf, G., Cochran, J. Applications of yeast surface display for protein engineering. *Methods Mol Biol*. **2015**, 1319, pp. 155-75.

[65] Pepper, L., Cho, Y., Boder, E., Shusta, E. A decade of yeast surface display technology: where are we now? *Comb Chem High Throughput Screen*. **2008**, 11(2), pp. 127-34.

[66] Sananes, A., Cohen, I., Shahar, A., Hockla, A., Vita, E., Miller, A., Radisky, E., Papo, N. A potent, proteolysis-resistant inhibitor of kallikrein-related peptidase 6 (KLK6) for cancer therapy, developed by combinatorial engineering. *J Biol Chem*. **2018**, pp. 1-33.

[67] Glotzbach, B., Reinwarth, M., Weber, N., Fabritz, S., Tomaszowski, M., Fittler, H., Christmann, A., Avrutina, O., Kolmar, H. Combinatorial optimization of cystine-knot peptides towards high-affinity inhibitors of human matriptase-1. *PLOS One*. **2013**, 8(10), pp. 1-10.

[68] Cohen, I., Kayode, O., Hockla, A., Sankaran, B., Radisky, D., Radisky, E., Papo, N. Combinatorial protein engineering of proteolytically resistant mesotrypsin inhibitors as candidates for cancer therapy. *Biochem J.* **2016**, 473(10), pp. 1329-41.

[69] Moghaddam-Taaheri, P. Protein and peptide engineering for improving therapies for applications in human health. PhD Thesis. University of Maryland. **2018**.

[70] Borg-von Zepelin, M., Beggah, S., Boggian, K., Sanglard, D., Monod M. The expression of the secreted aspartyl proteinases Sap4 to Sap6 from *Candida albicans* in murine macrophages. *Mol Microbiol.* **1998**, 28(3), pp. 543-54.

[71] Schild, L., Heyken, A., de Groot, P. W., Hiller, E., Mock, M., de Koster, C., Horn, U., Rupp, S., Hube, B. Proteolytic cleavage of covalently linked cell wall proteins by *Candida albicans* Sap9 and Sap10. *Eukaryotic Cell*. **2011**, 10(1), pp. 98-109.

[72] Huang, H., Gore, P., Shusta, E. Increasing yeast secretion of heterologous proteins by regulating expression rates and post-secretory loss. *Biotechnol Bioeng*. **2008**, 101(6), pp. 1264-75.

[73] Bochenska, O., Rapala-Kozik, M., Wolak, N., Aoki, W., Ueda, M. Kozik, A. The action of ten secreted aspartic proteases of pathogenic yeast *Candida albicans* on major human salivary antimicrobial peptide, histatin 5. *Acta Biochim Pol*. **2016**, 63(3), pp. 403-10.

[74] Donlan, R. Biofilms and device-associated infections. *Emerg Infect Dis.* **2001**, 7(2), pp. 277-81.

[75] Séon, L., Lavalle, P., Schaaf, P., Boulmedais, F. Polyelectrolyte multilayers: a versatile tool for preparing antimicrobial coatings. *Langmuir*. **2015**, 31(47), pp. 12856-72.

[76] Lichter, J., Vliet, K., Rubner, M. Design of antibacterial surfaces and interfaces: polyelectrolyte multilayers as a multifunctional platform. *Macromolecules*. **2009**, 42(22), pp. 8573-86.

[77] Gribova, V., Auzely-Velty, R., Picart, C. Polyelectrolyte multilayer assemblies on materials surfaces: from cell adhesion to tissue engineering. *Chem. Mater.* **2012**, 24(5), pp. 854-69.

[78] Tostanoski, L., Eppler, H., Xia, B., Zeng, X., Jewell, C. Engineering release kinetics with polyelectrolyte multilayers to modulate TLR signaling and promote immune tolerance. *Biomaterials Science*. **2019**, 7, pp. 798-808.

[79] Guo, Y., Geng, W., Sun, J. Layer-by-layer deposition of polyelectrolyte-polyelectrolyte complexes for multilayer film fabrication. *Langmuir*. **2009**, 25(2), pp. 1004-10.

[80] Karlsson, A., Flessner, R., Gellman, S., Lynn, D., Palecek, S. Polyelectrolyte multilayers fabricated from antifungal beta-peptides: design of surfaces that exhibit antifungal activity against *Candida albicans*. *Biomacromolecules*. **2010**, 11(9), pp. 2321-28.

[81] Raman, N., Lee, M., Palecek, S., Lynn, D. Polymer multilayers loaded with antifungal beta-peptides kill planktonic *Candida albicans* and reduce formation of fungal biofilms on the surfaces of flexible catheter tubes. *J Control Release*. **2015**, 191, pp. 54-62.

[82] Salim, N., Silikas, N., Satterthwaite, J., Moore, C., Ramage, G., Rautemaa, R. Chlorhexidine-impregnated PEM/THFM polymer exhibits superior activity to fluconazole-impregnated polymer against *Candida albicans* biofilm formation. *Int J Antimicrob Agents*. **2013**, 41(2), pp. 193-96.

[83] Kong, E. F., Tsui, C., Boyce, H., Ibrahim, A., Hoag, S. W., Karlsson, A. J., Meiller, T. F., Jabra-Rizk, M. A. Development and in vivo evaluation of a novel histatin-5 bioadhesive hydrogel formulation against oral candidiasis. *Antimicrob Agents Chemother*. **2015**, 60(2), pp. 881-89.

[84] Li, Q., Yi, L., Hoi, K., Marek, P., Georgiou, G., Iverson, B. Profiling protease specificity: combining yeast ER sequestration screening (YESS) with next generation sequencing. *ACS Chem Biol.* **2016**, 12(2), pp. 510-518.

[85] Etienne, O., Gasnier, C., Taddei, C., Voegel, JC., Aunis, D., Schaff, P., Meta-Boutique, M., Bellemin, A., Egles, C. Antifungal coating by biofunctionalized polyelectrolyte multilayer films. *Biomaterials*. **2005**, 26(33), pp. 6704-12.

[86] MacDonald, M., Rodriguez, N., Nisarg, S., Hammond, Paula. Characterization of Tunable FGF-2 Releasing Polyelectrolyte Multilayers. *Biomacromolecules*. **2010**, 11(8), pp. 2053-59.